Original Article

Characterization of The Decellularized Male Rabbit Kidney as A Three-Dimensional Natural Scaffold for Tissue Engineering. A Histological Study

Sara Abdel Gawad Elsebay, Ayat Abdelnaby, Gehan Khalaf and Naglaa Abou Rabia

Department of Histology and Cell Biology, Faculty of Medicine, Ain Shams University, Egypt

ABSTRACT

Background: Renal transplantation is the only curative treatment of end stage renal disease. Shortage of donated organs is one of many obstacles facing renal transplantation. Whole organ decellularization could offer a natural scaffold for engineering an immune-compatible kidney ready for transplantation. This study aimed to characterize the decellularized male rabbit kidney by evaluation of the structural integrity of extracellular matrix (ECM) components as a natural scaffold for tissue engineering.
Materials and Methods: Kidneys were harvested from ten male New Zealand White Rabbits (NZWR) of an average weight (1000- 1500 gm). Group I: the control group included the ten right kidneys; processed immediately for histological, immunohistochemical and electron microscopic examinations. Group II: the decellularization group included the ten left kidneys; harvested carefully after cannulation under anaesthesia and kept frozen until decellularization. At decellularization, kidneys were thawed, perfused with 0.5% Sodium dodecyl sulfate (SDS) for 5-6 hours at room temperature until kidneys were completely white. Decellularized kidneys were processed for histological, immunohistochemical and electron microscopic examinations.
Results: Decellularized kidney Scaffolds were entirely decellularized. The integrity of different extracellular matrix components, the ultrastructure and the three-dimensional (3D) structure of decellularized kidneys were generally preserved. However, the mean optical density of collagen type IV in kidney medulla and the thickness of Glomerular basement membranes were significantly affected.
Conclusion: The presented protocol demonstrated an efficient decellularization of male rabbit kidney. These results can pave the road for further investigations to move to the next step "recellularization".

Received: 11 July 2021, **Accepted:** 20 August 2021

Key Words: Decellularization, kidney, rabbit, sodium dodecyl sulfate.

Corresponding Author: Sara Elsebay, MSD, Department of Histology and Cell Biology, Faculty of Medicine, Ain Shams University, Egypt, **Tel.**: +20 10 6780 0614, **E-mail:** sara_elsebaey@med.asu.edu.eg

ISSN: 1110-0559, Vol. 45, No. 4

BACKGROUND

Chronic kidney disease (CKD) is an increasing global health problem and a leading cause of morbidity and mortality worldwide[1]. Global prevalence of CKD ranged between 10 and 16% of the adult population and increased up to 36% among high-risk populations[2]. Poverty and lower socioeconomic status have been considered risk factors for CKD and its progression into end stage renal disease (ESRD)[3]. Kidney transplantation stands still the favorable and potentially curable modality of treatment of ESRD when compared with dialysis, especially regarding the long-term outcomes and cost effectiveness[4,5]. Tissue engineering is a promising alternative to organ transplantation where an appropriate scaffold, cells and growth factors or signaling molecules can be used to engineer a functioning human tissue[6,7,8,9].

Whole organ decellularization is a promising technique for preparation of a 3D decellularized extracellular matrix (dECM) as natural scaffold that can be recellularized with the patient's own cells to produce a functional organ ready for transplantation[7,9]. Decellularization involves using chemical, enzymatic, physical or combinative methods for removal of the immunogenic cellular and genetic components, leaving behind the non-immunogenic ECM components[10] which does not elicit immune-mediated rejection, since ECM components are quite conserved across species[8]. The optimal decellularization protocol should preserve the 3D ultrastructure, vasculature, nanotopography, biophysical and biochemical properties of the resultant dECM scaffold[9]. Also, it should preserve ECM proteins; both native ECM structural proteins (e.g. collagens, laminins, fibronectin) and associated/ sequestrated ECM proteins (e.g. growth factors and cytokines)[10]. Therefore, the proper dECM can mimic the in *vivo* milieu of cells and modulate their behavior (attachment, migration, signaling, proliferation and differentiation) during recellularization[8]. Also, the dECM can direct the differentiation of stem cells towards certain linages[11]. Thus, dECM is the closest scaffold to

 DOI: 10.21608/ejh.2021.84255.1524

nature and it can be considered the gold standard natural 3D scaffolds[12].

MATERIALS AND METHODS

An experimental randomized control study was conducted to characterize the decellularized male rabbit kidney by evaluation of the structural integrity of ECM components as a natural scaffold ready for tissue engineering. Ten male NZWR of average weight (1000-1500 gm) were purchased from a nearby local market and were housed in the Medical Research Centre, Faculty of Medicine, Ain Shams University for at least seven days before harvesting kidneys for acclimatization. NZWR were kept under proper conditions of light, temperature and humidity in clean plastic cages with mesh wire covers and were given a free access to standard diet and tap water[13]. All animal procedures were performed in accordance with the animal care and use guidelines of Scientific Research Ethics Committee of Faculty of Medicine, Ain Shams University.

Harvesting kidneys

The operations of harvesting kidneys were performed at the Medical Research Centre, Faculty of Medicine, Ain Shams University. Each Rabbit was sedated with Ketamine 25-50 mg/kg intramuscularly (Ketamine®, Sigma Tec Pharmaceutical Industries, Egypt), while the rabbit was still in familiar surroundings to decrease stress[13]. Then, it was brought to operation theatre and anaesthetized using Thiopental 30 mg/kg (Anapental®, Sigma Tec Pharmaceutical Industries, Egypt) intravenously (IV) through a 24- gauge intravenous (IV) cannula secured in the auricle[13]. After that, 100 units IV bolus of Unfractioned Heparin (Cal-Heparin 5000 IU/mL amp, Amoun, Egypt) were given through the cannula[14].

A central abdominal incision was made and kidneys, aorta, vena cava, and ureters were identified. The kidneys were harvested into two groups. Group I (Control group); included the ten right kidneys of the ten rabbits as a negative control group. Group II (Decellularization group); included the ten left kidneys of the ten rabbits.

The left kidneys (Decellularization group kidneys) were harvested first as follows: The vascular pedicle of the left kidney was opened carefully to separate the left renal artery from the left renal vein. The left main renal artery was cannulated with a 24- gauge IV cannula secured with a 4/0 silk suture. Caution was taken not to ligate the left renal vein in the process. Then, the left kidney was perfused with phosphate buffered saline (PBS) (Sigma-Aldrich Co. Lot number:SLBD7938); prepared by dissolving dry powder pouch in 1-liter distilled water yielding 0.01 M PBS; pH 7.4) until blanching to remove residual blood. The cannulated kidney was then harvested carefully, placed in an empty petri dish and weight (fresh kidney weight) was recorded using an electronic scale (ACB plus-300 ADAM®- Adam Lab). The petri dish was then filled with PBS and kept frozen at -80°C for 1-2 weeks until decellularization.

After that, the right kidneys (control group kidneys) were dissected out and processed immediately for examination. All rabbits were then sacrificed with ether inhalation. The bodies of dead rabbits were disposed using an incinerator.

Whole organ decellularization procedures

The procedures were performed at the Stem Cell Research Unit, Histology and Cell Biology Department, Faculty of Medicine, Ain Shams University. Each left kidney was thawed at room temperature and its weight was recorded (weight after freezing/thawing).

The cannulated kidney was connected through an IV line to a 50 mL plastic syringe applied to a peristaltic pump (hawkmed® HK-400II syringe pump) by (Shenzhen Hawk Optical Electronic Instrument CO., LTD.) (Figure 1). The kidney was perfused with PBS to remove residual blood at infusion rate 3 mL/min for 30 min until a clear fluid came out from the renal vein. Then, the kidney was decellularized using 0.5 w/v SDS; prepared by adding 5 grams of SDS (Sigma- Aldrich) powder to 1000 mL PBS at room temperature. A magnetic stirrer (AGE magnetic stirrer, VELP® scientifica) was used until the SDS crystals dissolved completely. SDS was perfused for 5-6 hours at room temperature until the kidney was completely white. Infusion rate started at 3 mL/min and was incrementally increased 1 mL per hour till reaching 7-8 mL/min at the end. Finally, the kidney was perfused with PBS for 2 hours to wash out the SDS residues. The weight was recorded (weight after complete decellularization). The decellularized kidneys were then processed for examination.

Fig. 1: A photograph showing the decellularization device assembled by connecting the cannulated left rabbit kidney to hawkmed® HK-400II syringe pump (Shenzhen Hawk Optical Electronic Instrument CO., LTD) which infuse fluids at certain given rates. On the left, a closer view showing the IV cannula inserted in the renal artery (A) while the renal vein (V) and ureter (U) are free.

Kidney Specimen Processing for Examination and Analysis

Each kidney of both groups was divided transversely into small upper part to be fixed immediately in 2.5% formol-glutraldehyde to be processed for electron microscopic examination. The larger lower part was cut sagittally, fixed immediately in 10% neutral buffered

formalin, dehydrated, cleared and embedded in paraffin. 5 µm sagittal sections were obtained and processed for histological and immunohistochemical examinations[15].

For histological examination, sections were stained with H&E, Feulgen nuclear reaction, modified McManus periodic acid Schiff's technique (PAS), combined alcian blue-PAS technique, modified Masson′s trichrome stain, Gordon & Sweets' silver impregnation method[15] and orcein stain[16].

For immunohistochemical examination, sections were stained with immunoperoxidase labeled streptavidin-biotin complex technique for detection of laminin, fibronectin and collagen type IV. Briefly, sections were properly dewaxed in xylene, rehydrated in descending grades of alcohol. Endogenous peroxidase activity was blocked followed by Avidin biotin blocking. Heat-mediated antigen retrieval was carried out. Then, sections were blocked with 1/200 normal goat serum. These steps were the same for all sections. After that, sections were incubated with the primary antibody followed by the secondary antibody. For detection of laminin, (1:100) rat anti-rabbit laminin beta-2/gamma-1 monoclonal antibody (A5), In*vitro*gen by Thermo Fisher Scientific, catalog: (MA5-14649) was used as the primary antibody, followed by (1:500) goat anti-rat IgG (H+L) secondary antibody, Biotin, In*vitro*gen by Thermo Fisher Scientific, catalog: (31830). For detection of fibronectin, (1:500) mouse anti-rabbit fibronectin monoclonal antibody (FBN11), In*vitro*gen by Thermo Fisher Scientific, catalog: (MA5-11981) was used, followed by (1:200) goat anti-mouse IgG (H+L) cross-adsorbed secondary antibody, Biotin, In*vitro*gen by Thermo Fisher Scientific, catalog: (62-6540). For detection of collagen type IV, (1:50) mouse anti-rabbit collagen IV monoclonal antibody (CIV 22), In*vitro*gen by Thermo Fisher Scientific, catalog: (MA5-13437), followed by (1:200) goat anti-mouse IgG (H+L) cross-adsorbed secondary antibody, Biotin, In*vitro*gen by Thermo Fisher Scientific, catalog: (62-6540). Then, sections were incubated with peroxidase labelled streptavidin-biotin complex (ABC peroxidase staining kit, Thermoscientific, catalog Number: 32020). After washing with PBS, positive reaction was visualized by incubating sections with 3, 3'-Diaminobenzidine; (eBioscience™ DAB Advanced Chromogenic Kit, In*vitro*gen by Thermo Fisher Scientific, catalog number: 8801-4965). Finally, nuclei were counterstained with hematoxylin. Negative controls were prepared by replacing the primary antibody with PBS[15].

For transmission electron microscopic examination (TEM), 0.5–1.0 mm3 samples fixed immediately in 2.5% formol-glutaraldehyde for 24 hours at 4°C, were rinsed properly in PBS. Then, samples were post-fixed in 1% osmium tetroxide for 60–90 minutes at room temperature. Again, samples were rinsed properly in PBS. After that samples were dehydrated gradually in ascending grades of alcohol, cleared in propylene oxide and infiltrated with ascending concentrations of liquid resin/propylene ethanol over 2 hours. Then, samples were left in pure resin for 24 hours at room temperature. Finally, samples were embedded in fresh Epon resin to be polymerized at 60-70 °C for 48 hours. 1 µm thick semi-thin sections were obtained, stained with 1% toluidine blue for light microscopic examination. Ultra-thin sections cut at 60 nm were stained with uranyl acetate and lead citrate to be examined with transmission electron microscope (JEOL- JEM- 1200EX II- Electron Microscope) in the Electron Microscopy Unit, Faculty of Science, Ain Shams University, Cairo, Egypt[15].

For scanning electron microscopic examination (SEM), 0.5 cm3 samples were processed the same way as the TEM regarding fixation, post-fixation and dehydration. Then, the samples were placed in acetone for 15 minutes. Critical point drying was performed as described in the instruction manual of the critical point dryer apparatus. After that, samples were mounted on a stub with a double-sided sticky tape, sputtered with gold palladium in a sputter coater and examined with (JEOL- JSM- 5500LV) SEM at the regional center for mycology and biotechnology, El-Azhar University, Cairo, Egypt[17].

Morphometric measurements and statistical analysis

Morphometric measurements were taken at Image Analysis Unit, Histology and Cell Biology Department, Faculty of Medicine, Ain Shams University using image analyzer Leica Q win V3 Program and a Leica DM2500 microscope (Wetzlar, Germany). All the following measurements were expressed as mean± standard deviation in both cortex and medulla.

a. Area percentage of green collagen fibers in Masson's trichrome stained sections.

b. Area percentage of reticular fibers in Gordon and sweets silver impregnation stained sections.

c. Area percentage of internal elastic laminae of arcuate arteries in orcein stained sections.

d. Optical density of glycoproteins or positive PAS reaction in PAS stained sections.

e. Optical density of glycosaminoglycans (GAGs) or positive alcian blue reaction in alcian blue-PAS stained sections.

f. Optical density of laminin positive reaction using anti-laminin antibody stained sections.

g. Optical density of fibronectin positive reaction using anti-fibronectin antibody stained sections.

h. Optical density of collagen IV positive reaction using anti-collagen IV antibody stained sections.

Statistical analysis

Was carried out using IBM SPSS statistics software package (version 20, IBM co., New York, USA). Independent samples T-test was performed to look for statistically significant differences between the means of all morphometric measurements of both groups. Also, the independent samples T-test was used to look for

the significant differences between the mean thickness of Glomerular basement membranes (GBMs) of both groups measured during TEM examination of ultrathin sections. In addition, One-way analysis of variance (one- way ANOVA) test was performed to look for statistically significant differences between the mean weight of kidneys of decellularization group II (fresh weight, weight after freezing/thawing and weight after complete decellularization). The significance of data was determined by the *P. value* (probability of chance) where; ($P > 0.05$) was insignificant, ($P < 0.05$) was significant and ($p < 0.001$) was highly significant.

RESULTS

Gross Results

Eight successful decellularization procedures produced a completely white kidney dECMs. Two failed trials occurred due to false insertion of the cannula into the renal artery or displacement of the cannula and laceration of the artery during attempts of reinsertion. These two kidneys were excluded from further examination and analysis.

At the beginning, kidneys were reddish brown. PBS infusion caused blanching of the kidneys. Immediately after SDS infusion, multiple tiny semi-transparent areas started to appear all over the kidneys. These semi-transparent areas grew gradually in both size and number until the whole cortex was semi-transparent. The kidney medulla was still seen as a deep pinkish area underneath the decellularized cortex. By time, the medulla became semi-transparent gradually. The arborization of the kidney vasculature could be easily seen underneath the transparent kidney capsule (Figure 2).

The recorded weight data of decellularization group (group II) showed two steps decrease in the mean weight. The freezing/thawing step caused ≈ 2.3% decrease in the mean weight. SDS infusion caused ≈ 43.1% decrease in the mean weight. A total ≈ 45.4 % decrease in the mean weight was recorded. Statistical analysis showed no significant difference ($P > 0.05$) between the mean fresh kidney weight and the mean weight after freezing/ thawing, while there was a highly significant difference ($P < 0.001$) between mean fresh kidney weight and mean weight after complete decellularization (Figure 3).

Histological Results

Histological examination of H&E stained sagittal sections of control group I showed the architecture of the unipyramidal rabbit kidney; formed of an outer cortex and an inner medulla. The cortex was distinguished by having numerous renal corpuscles surrounded by closely packed profiles of proximal and distal convoluted tubules. Groups of straight tubules radiated from the medulla towards the cortex forming the medullary rays. Each Renal corpuscle formed of a glomerulus supported by mesangial cells and surrounded by the visceral and parietal layers of the Bowman's capsule. The podocytes forming the visceral layer of the capsule were seen in intimate relation with the glomerulus, while the simple squamous epithelial cells lining the parietal layer were separated by the urinary space. Most profiles of convoluted tubules belonged to the long and highly tortuous proximal convoluted tubules (PCTs), while the profiles of the distal convoluted tubules (DCTs) were apparently less numerous. Other tubular profiles seen in the cortex belonged to the straight tubules and cortical collecting ducts within the medullary rays (Figure 4;a).

The unipyramidal medulla was marked by numerous profiles of tubules and ducts that ran towards the tip of the renal pyramid, the renal papilla. Different types of medullary tubules were recognized; the proximal and distal thick segments of loop of Henle, the thin segments of loop of Henle. These tubules were drained by the medullary collecting ducts, then by the papillary ducts (of Bellini). Numerous profiles of the straight blood vessels (vasa recta) were seen in-between the medullary tubules and ducts. The amount of the interstitial tissue between the renal tubules increased gradually in the direction of the renal papilla (Figures 4 c,e).

Histological examination of H&E stained sagittal sections of decellularization group II showed that the outline of kidneys' architecture was preserved. There was total loss of nuclear basophilia. The outline of renal corpuscles appeared conserved as the lumina of their glomeruli were patent and their basement membranes were seen intact. Numerous profiles of convoluted tubules were seen with intact basement membranes but with total loss of their lining cells. Thus, the PCTs and the DCTs could not be distinguished from each other (Figure 4 b). Similarly, the medulla was preserved with total loss of nuclear basophilia. Characteristic cells lining the medullary tubules and ducts were completely lost (Figures 4 d,f).

Examination of Feulgen nuclear reaction stained sections of control group I showed a positive magenta red reaction of nuclei of kidney cells against a green background in the cortex (Figure 5a) and medulla (Figure 5 b). While examination of Feulgen nuclear reaction stained sections of decellularization group II showed no nuclear reaction in the cortex (Figure 5 c) and medulla (Figure 5 d).

Examination of the PAS stained sections of control group I showed a well-defined PAS positive reaction of GBMs, basement membranes of the parietal layer of Bowman′s capsule (Figure 6 a). Tubular basement membranes showed a well-defined PAS positive reaction. The cells of the PCTs and the proximal straight tubules also exhibited PAS positive apical brush borders (Figures 6 a,b).

The decellularization group II also exhibited a well-defined PAS positive reaction of GBMs (Figure 6 c) and tubular basement membranes (Figures 6 c,d). The basement membranes were seen intact with complete loss of lining cells. Loss of characteristic cells lining the tubules and ducts didn't allow their identification (Figures 6 c,d). In addition, there was no significant difference ($P > 0.05$) between mean optical density of glycoproteins in renal

cortex and medulla of control group and those of cortex and medulla of decellularization group (Figure 7).

Examination of combined Alcian blue–PAS stained sections of control group I showed that GBMs (Figure 8 a), tubular basement membranes (Figures 8 a,b) exhibited both positive Alcian blue and PAS reactions (appeared as different shades of the purple color; a mixture of Alcian blue and PAS) denoting the presence of GAGs and glycoproteins respectively. The apical cell membranes of epithelial cells lining renal tubules also showed both positive Alcian blue and PAS reaction on the apical cell surfaces. But the apical cell surface of the PCTs and their straight counterparts (the proximal straight tubules) had a stronger positive PAS reaction due to presence of the brush borders. In addition, the interstitium and connective tissue of the walls of renal vasculature exhibited both positive Alcian blue and PAS reactions (Figures 8 a,b).

The examination of decellularization group II showed preservation of GAGs and glycoproteins distribution in both renal cortex and medulla. Positive Alcian blue and PAS reactions were seen in GBMs, tubular basement membranes, renal interstitium and walls of blood vessels. But complete loss of cells caused loss of GAGs and glycoproteins attached to apical cell membranes (Figures 8 c,d). Furthermore, the statistical analysis revealed that there was no significant difference ($P > 0.05$) between mean optical density of GAGs in both renal cortex and medulla of control group and those of decellularization group (Figure 9).

Masson's trichrome stained sections of control group I showed few scattered collagen fibers around the glomerular capillaries, the renal corpuscles (Figure 10 a) and the renal tubules (Figure 10 a,b,c). Also, collagen fibers were seen in the walls of renal blood vessels and in the connective tissue of kidney capsule (Figure 10 a). The amount of interstitial tissue and the amount of collagen fibers exhibited an apparent and gradual increase from cortex towards medulla.

Examination of Masson's trichrome stained sections of decellularization group II showed preservation of the distribution of collagen fibers all over the kidney. Collagen fibers were observed in between the glomerular capillaries, the renal tubules and in the walls of the renal blood vessels. Neither cells and their nuclei, nor cellular debris were seen. The amount of interstitial tissue and the amount of collagen fibers were apparently increased gradually from cortex towards the medulla (Figures 10 d,e,f). In addition, there was no significant difference ($P > 0.05$) between mean area percentage of collagen fibers in renal cortex and medulla of control group and those of decellularization group (Figure 11).

Examination of Gordon & Sweets' silver impregnation stained sections of control group I revealed that reticular fibers filled the background/interstitial spaces of the control kidneys and took the shape of their parenchyma. The amount of interstitial tissue and the amount of reticular fibers apparently increased from cortex (Figure 12 a) towards medulla (Figures 12 b,c). The highest amount was seen at the renal papilla.

Examination of decellularization group II revealed preservation of the histological distribution of reticular fibers in cortex (Figure 12 d) and medulla (Figure 12 e,f) that took the shape of the parenchyma even after complete cell removal. Statistical analysis of morphometric measurements showed that there was no significant difference ($P > 0.05$) between mean area percentage of reticular fibers in renal cortex and medulla of control group and those of decellularization group (Figure 13).

Microscopic examination of orcein stained sections of control group I showed that elastic fibers were minimal in the ECM of rabbit kidneys. Reddish brown elastic fibers were seen mainly in the walls of renal blood vessels. Also, internal elastic laminae were seen as continuous wavy reddish-brown sheets in the intima of small renal arteries and arterioles (Figure 14 a).

Orcein stained sections of decellularization group II revealed preserved intact internal elastic laminae in the intima of small renal arteries and arterioles. Also, fine elastic fibers were seen in the adventitia of these arteries (Figure 14 b). Statistical analysis revealed that there was no significant difference ($P > 0.05$) between the mean area percentage of internal elastic laminae of arcuate arteries of control group and those of decellularization group (Figure 15).

Immunohistochemical results

Microscopic examination of anti-laminin antibody stained sections of control group I showed no immunohistochemical reaction for laminin and no background staining of the negative control section (Figure 16 a). On the contrary, the positive control sections of the cortex showed positive immunohistochemical reaction for laminin in the GBMs and tubular basement membranes (Figure 16 b). Also, basement membranes of medullary tubules and ducts showed positive immunohistochemical reaction for laminin (Figure 16 c).

Examination of anti-laminin antibody stained sections of decellularization group II showed preserved distribution of laminin in the GBMs, tubular basement membranes, basement membranes of endothelial cells and basal laminae of smooth muscle fibers of the walls of renal blood vessels (Figure 16 d,e). In addition, there was no significant difference ($P > 0.05$) between mean optical density of laminins in both renal cortex and medulla of control group and that of decellularization group (Figure 17).

Examination of anti-fibronectin antibody stained sections of control group I showed no immunohistochemical reaction for fibronectin and no background staining of the negative control section (Figure 18 a). On the other hand, positive control sections showed positive immunohistochemical reaction for fibronectin in the GBMs and the mesangium around glomerular capillaries

(Figure 18 b). Also, positive anti-fibronectin reaction was seen in the tubular basement membranes and the interstitium around renal tubules together known as tubulointerstitium. In addition, the connective tissue of the walls of renal blood vessels showed positive reaction for fibronectin (Figures 18 b,c).

Examination of anti-fibronectin antibody stained sections of decellularization group II showed preserved distribution of fibronectin in the in GBMs, the mesangium, the tubulointerstitium and in the connective tissue of the vascular walls. (Figures 18 d,e). In addition, there was no significant difference ($P > 0.05$) between mean optical density of fibronectin in both renal cortex and medulla of control group and that of decellularization group (Figure 19).

Examination of anti-collagen IV antibody stained sections of control group I showed that the negative control sections exhibited no reaction for collagen IV and no background staining (Figure 20 a). Otherwise, the positive control sections showed positive immunohistochemical reaction for collagen IV in the GBMs (Figure 20 b) and in tubular basement membranes (Figure 20 c).

Examination of anti-collagen IV antibody stained sections of decellularization group II showed preserved distribution of collagen IV in the GBMs (Figure 20 d), tubular basement membranes (Figures 20 d,e). In addition, there was no significant difference ($P > 0.05$) between mean optical density of collagen IV in renal cortex of control group and that of decellularization group. But, there was a significant difference ($P < 0.05$) between mean optical density of collagen IV in medulla of control group and that of decellularization group (Figure 21).

Toluidine blue stained semithin sections

Examination of toluidine blue stained semithin sections of cortices of control group I showed multiple renal corpuscles surrounded by numerous profiles of convoluted tubules. Renal corpuscles were formed of tuft of glomerular capillaries surrounded by podocytes forming the visceral layer of Bowman's capsule. The parietal layer was lined by flat epithelial cells. In between the glomerular capillaries, mesangial cells were seen surrounded by mesangial matrix (Figure 22 a). PCTs were distinguished easily from DCTs by having larger outer diameters, narrower lumina and fewer lining cells. Also, PCTs had apical brush borders almost masking their lumina while DCTs hadn't (Figure 22 b).

Toluidine blue stained semithin sections of cortices of decellularization group II showed completely decellularized renal corpuscles surrounded by numerous completely decellularized profiles of convoluted tubules. Only the GBMs and tubular basement membranes were seen with complete loss of lining cells (Figures 22 c,d).

Transmission electron microscopic results

Transmission electron microscopic examination of cortices of control group I showed fenestrated endothelial cells lining the walls of glomerular capillaries and resting on a thick glomerular basement membrane (GBM). The GBM was shared between multiple capillaries. It surrounded the endothelial cells completely except where mesangial cells were present (Figure 23 a). The thick GBM resulted from fusion of both basal laminae of endothelial cells and podocytes foot processes covering the outer surface of the GBM. Thus, GBM was seen formed of three laminae; two electron lucent laminae rara externa and interna and in between an electron dense lamina densa. Thin filtration slit diaphragms were seen spanning the filtration slit pores between the interdigitating foot processes of podocytes. (Figure 23 b).

TEM examination of decellularization group II showed preserved ultrastructural profile of decellularized kidney cortices. Lumina of glomerular capillaries were seen patent. Endothelial cells and podocytes were completely lost (Figure 23 c). GBMs were seen intact but the three laminae of the GBMs couldn't be seen clearly (Figure 23 d).

In addition, statistical analysis of GBMs thickness measurements showed that there was a significant difference ($P < 0.05$) between the mean thickness of GBMs of control group and those of decellularization group (Figure 24).

Scanning electron microscopic results

Scanning electron microscopic examination of control group I showed the two distinct structural arrangements of renal cortex; the pars convoluta (the cortical labyrinth) containing renal corpuscles surrounded by convoluted tubules and the pars radiata (medullary rays) containing longitudinal straight tubules and cortical collecting ducts. Each renal corpuscle was seen formed of loops of glomerular capillaries surrounded by the double layered Bowman's capsule (Figure 25 a). The visceral layer was formed of podocytes covering intimately the capillary loops of the glomerulus. Podocytes extended complex interdigitating primary, secondary, and tertiary processes to cover the entire capillary surfaces. Slit-like filtration pores were seen between the interdigitating tertiary processes. The parietal layer was separated from the visceral layer by the urinary space. Cross sections of renal tubules were seen having an apparently thicker wall than the decellularization group (Figure 25 b).

SEM examination of decellularization group II showed preserved 3D architecture of renal cortex. Some renal corpuscles were seen surrounded by intact Bowman's capsules. When a capsule was opened, the glomerulus inside the corpuscle was seen formed of intact capillary loops. The podocytes and their interdigitating foot processes forming the visceral layer of Bowman's capsule were absent. Cross sections of renal tubules and collecting ducts were seen having a very thin wall representing their basal laminae after complete loss of their lining cells (Figure 25 c).

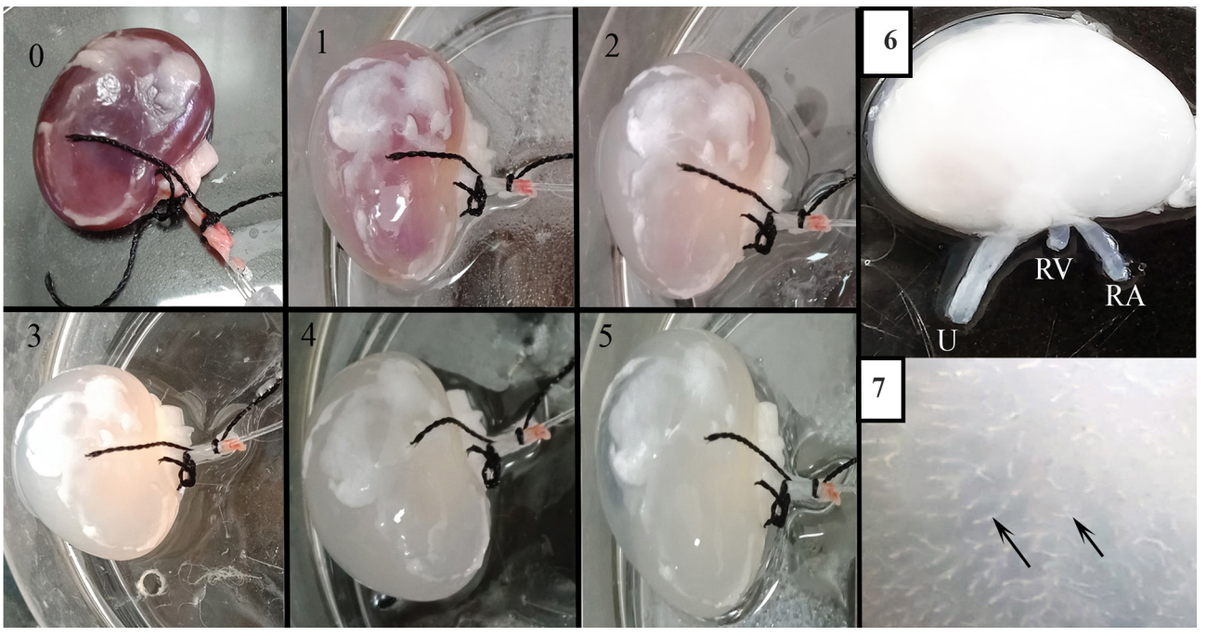

Fig. 2 (0:7): photographs showing gross morphological changes of a kidney of group II during decellularization. (0) the kidney is reddish brown after freezing/thawing and before starting SDS infusion. (1), (2), (3), (4) and (5) represent the changes after the 1st, 2nd, 3rd, 4th and 5th hour of SDS infusion respectively. The photograph (6) -at the end of decellularization- shows a completely white kidney. The renal artery (RA), renal vein (RV) and the ureter (U) are seen intact at the hilum of the kidney. A closer view (7) shows the arborization of the vascular tree (↑).

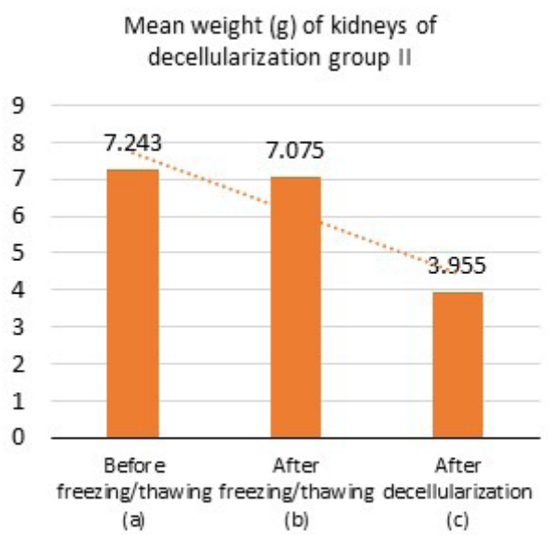

Fig. 3: A charts showing mean weight of kidneys of decellularization group II (Before freezing/thawing, after freezing/thawing and after decellularization).

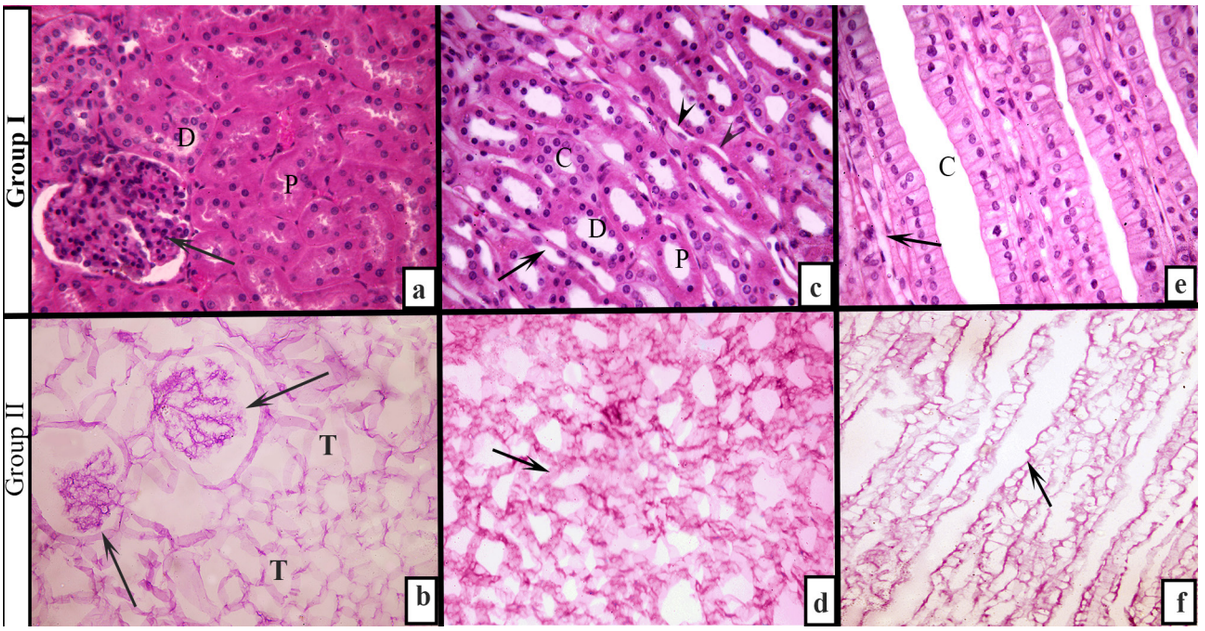

Fig. 4 (a:f): Photomicrographs of sagittal sections of rabbit kidneys. [a] Cortex of control group I showing a glomerulus (↑) seen inside its renal corpuscle and surrounded by numerous closely packed profiles of proximal (P) and distal (D) convoluted tubules. [b] Cortex of decellularization group II sowing two glomeruli (↑) seen intact inside their corpuscles. The surrounding profile of renal tubules (T) have intact basement membranes with total loss of the lining cells and their nuclei. [c] Outer medulla of control group I showing numerous profiles of proximal (P) and distal (D) medullary straight tubules, collecting ducts (C), thin segments of loop of Henle (↑) and vasa recta (▲). [d] Outer medulla of decellularization group II showing only the basement membranes (↑) of different medullary structures while their lining cells are completely lost. [e] Inner medulla of control group I showing medullary collecting ducts (C) and thin segments of loop of Henle (↑). [f] Inner medulla of decellularization group II showing basement membranes (↑) of medullary ducts and tubules seen intact with total loss of lining cells and their nuclei. (H&E x400)

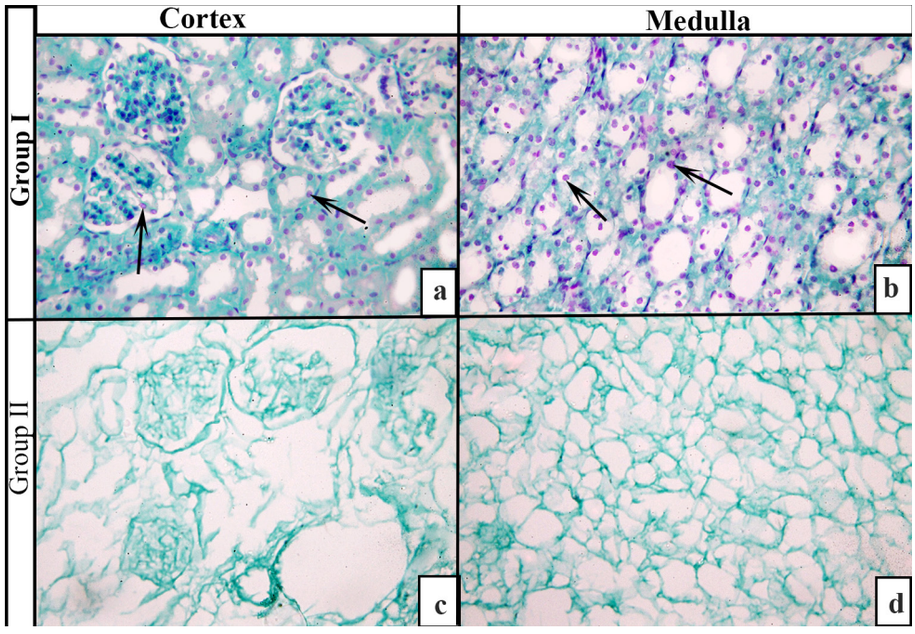

Fig. 5 (a:d): Photomicrographs of rabbit kidneys. [a] Cortex and [b] medulla of control group I showing positive magenta red Feulgen nuclear reaction of nuclei (↑) against green backgrounds. [c] Cortex and [d] medulla of decellularization group II showing no Feulgen nuclear reaction while the green backgrounds express the general outline of renal tissue. (Feulgen nuclear reaction x400)

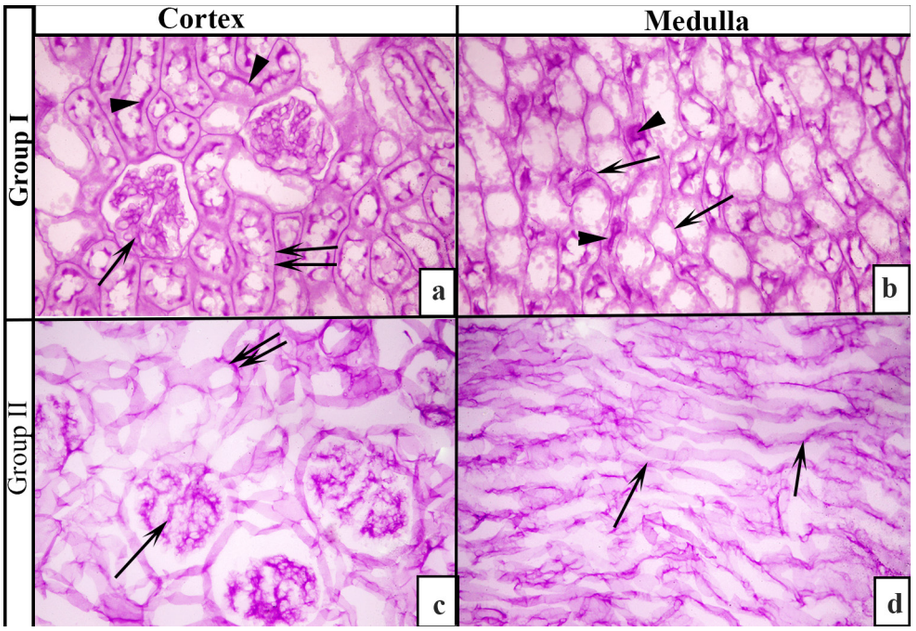

Fig. 6 (a:d): Photomicrographs of rabbit kidneys. [a] Cortex of control group I showing a well-defined PAS positive reaction of GBMs (↑) and basement membranes of convoluted tubules (↑↑). Also, a positive PAS reaction is seen at the apical brush borders of proximal convoluted tubules (▲). [b] Medulla of control group I showing a well-defined PAS positive reaction of basement membranes of medullary structures (↑). The proximal straight tubules show positive PAS apical brush borders as their convoluted counterparts (▲). [c] Cortex of decellularization group II showing intact PAS positive GBMs (↑) and basement membranes of convoluted tubules (↑↑). [d] Medulla of decellularization group II showing intact PAS positive basement membranes of medullary structures (↑). (PAS x400)

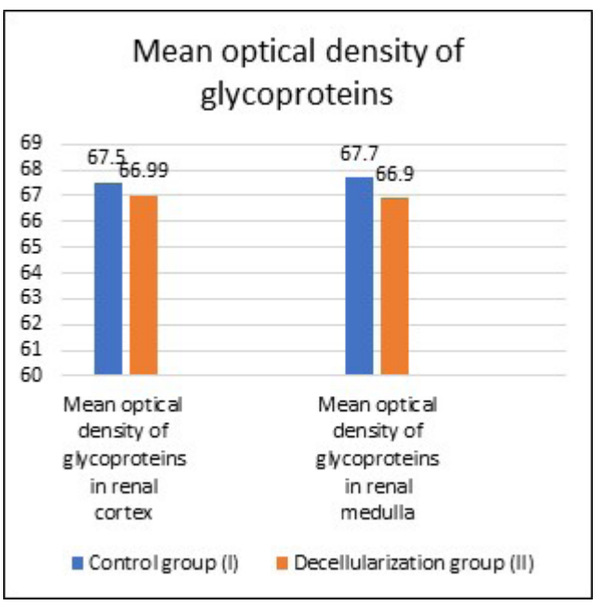

Fig. 7: A chart showing mean optical density of glycoproteins in both renal cortex and medulla of both control and decellularization groups.

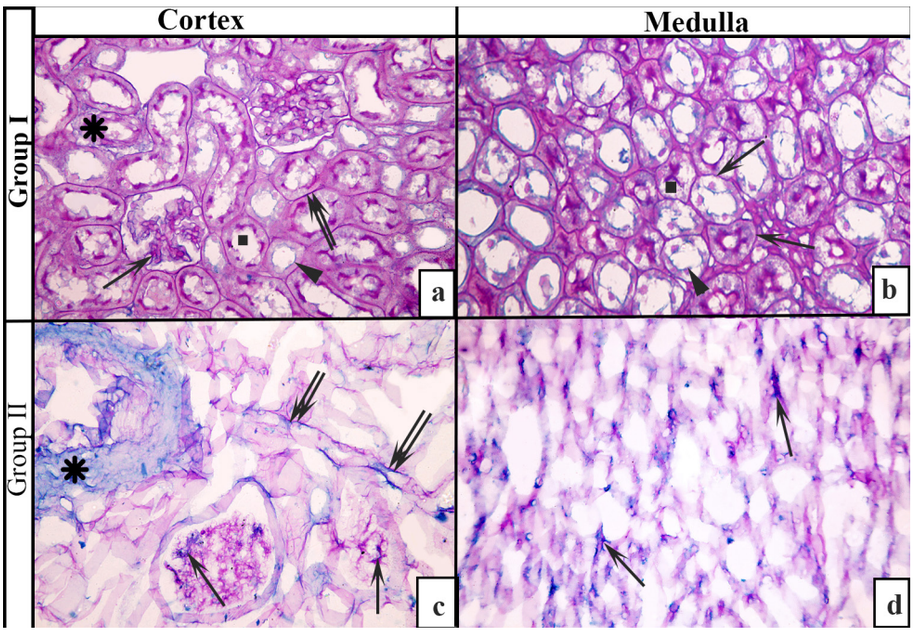

Fig. 8 (a:d): Photomicrographs of rabbit kidneys. [a] Cortex of control group I showing both positive Alcian blue and PAS reaction [seen as different shades of purple] of GBMs (↑), basement membranes of convoluted tubules (↑↑) and walls of cortical blood vessels(*). The apical cell membranes of convoluted tubules (▲) also exhibit both positive Alcian blue and PAS reaction, but the apical brush borders of the proximal convoluted tubules (■) show a stronger PAS reaction than the distal tubules. [b] Medulla of control group I showing both positive Alcian blue and PAS reaction of basement membranes of medullary straight tubules and collecting ducts (↑). The apical membranes of the straight tubules (▲) exhibit both positive Alcian blue and PAS reaction, but the apical brush borders of proximal straight tubules (■) show a stronger PAS reaction than the distal tubules. [c] Cortex of decellularization group II showing both positive Alcian blue and PAS reaction of GBMs (↑), basement membranes of convoluted tubules (↑↑) and walls of cortical blood vessels (*). [d] Medulla of decellularization group II showing both positive Alcian blue and PAS reaction of basement membranes of medullary straight tubules and collecting ducts (↑). (Combined Alcian-PAS x400)

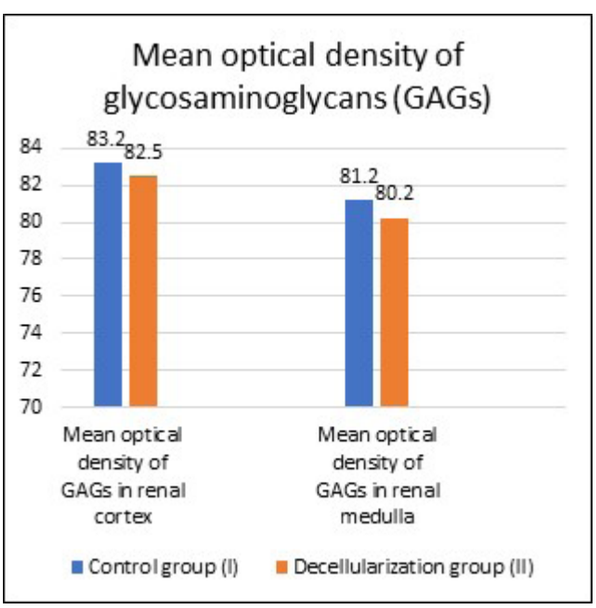

Fig. 9: A chart showing mean optical density of glycosaminoglycans (GAGs) in both renal cortex and medulla of both control and decellularization groups.

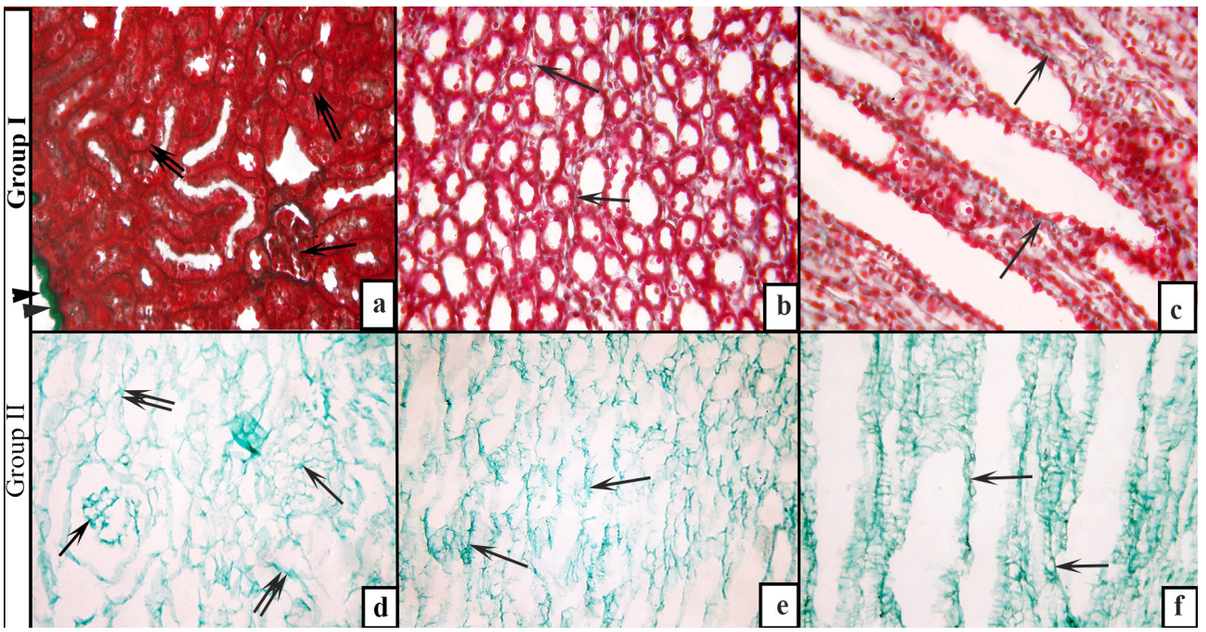

Fig. 10 (a:f): Photomicrographs of rabbit kidneys. [a] Cortex of control group I showing few green collagen fibers present in between glomeruli capillaries (↑) and cortical tubules (↑↑). Also, Green collagen fibers are seen in kidney capsule (▲). [b] Outer medulla of control group I showing few green collagen fibers present in between medullary tubules and ducts (↑). [c] Inner medulla of control group I showing green collagen fibers present in between medullary tubules and ducts (↑). [d] Cortex of decellularization group II showing preserved distribution of collagen fibers; the green collagen fibers are seen in glomeruli (↑) and in between cortical tubules (↑↑). [e] Outer medulla of decellularization group II showing preserved distribution of collagen fibers seen in between medullary tubules and ducts (↑). [f] Inner medulla of decellularization group II showing preserved distribution of collagen fibers seen in between medullary tubules and ducts (↑). (Masson's trichrome x400)

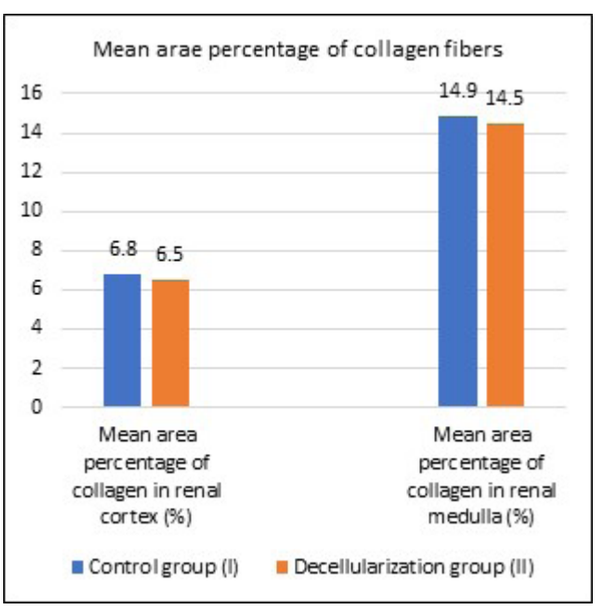

Fig. 11: A chart showing mean area percentage of collagen fibers in both renal cortex and medulla of both control and decellularization groups.

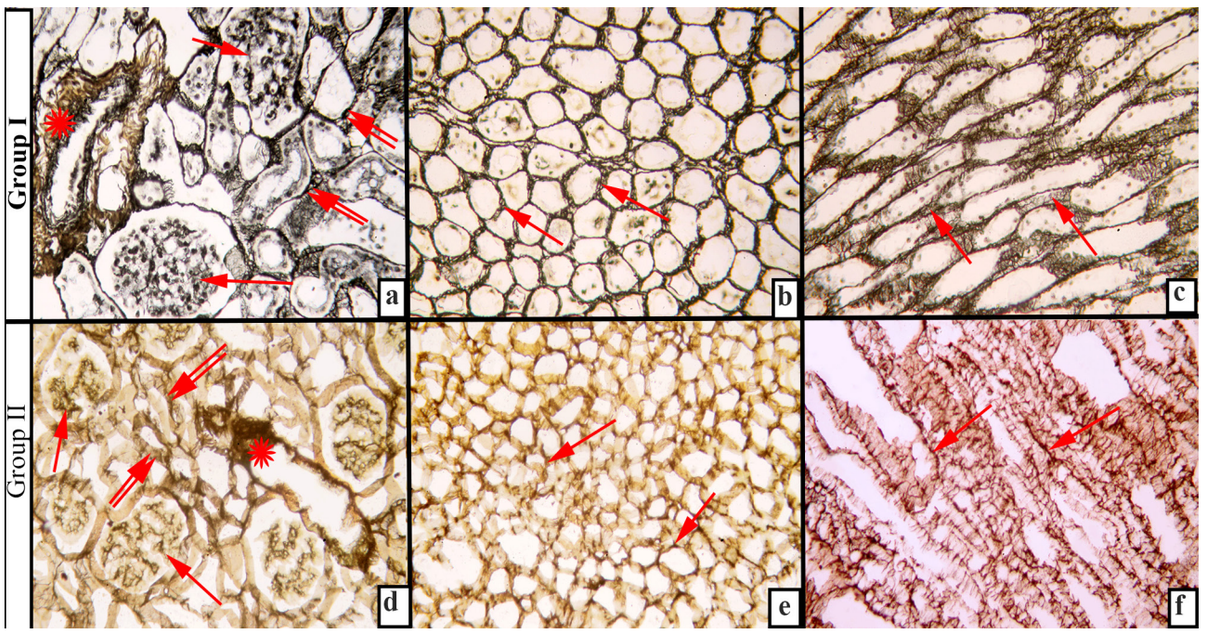

Fig. 12 (a:f): Photomicrographs of rabbit kidneys. [a] Cortex of control group I showing black reticular fibers filling the background of the cortex and taking the shape of the renal corpuscles (↑), cortical tubules (↑↑) and cortical blood vessels (*). [b] Outer medulla of control group I showing black reticular fibers filling the background and taking the shape of medullary tubules and ducts (↑). [c] Inner medulla of control group I showing black reticular fibers filling the background and taking the shape of medullary structures (↑). [d] Cortex of decellularization group II showing preserved distribution of reticular fibers; the deep brown reticular/black fibers fill the background of the cortex and taking the shape of the renal corpuscles (↑), cortical tubules (↑↑) and cortical blood vessels (*). [e] Outer medulla of decellularization group II showing preserved distribution of reticular fibers seen in between medullary tubules and ducts (↑). [f] Inner medulla of decellularization group II showing preserved distribution of reticular fibers; they are seen filling the background of the medullary tubules and ducts (↑). (Gordon & Sweets' Silver Impregnation x400)

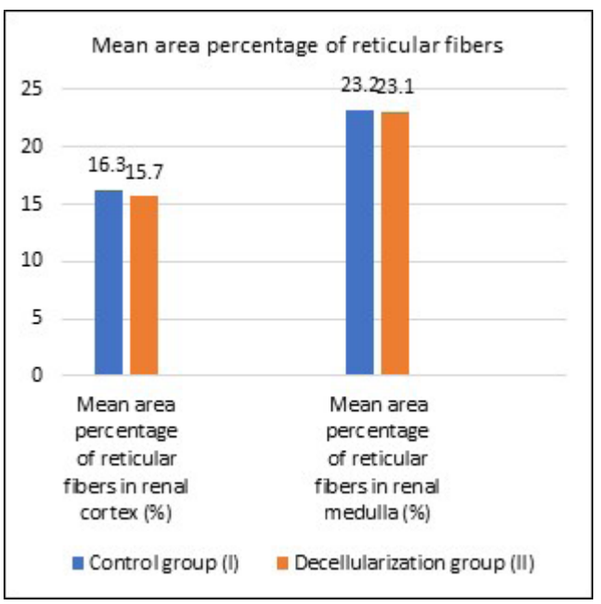

Fig. 13: A chart showing mean area percentage of reticular fibers in both renal cortex and medulla of both control and decellularization groups.

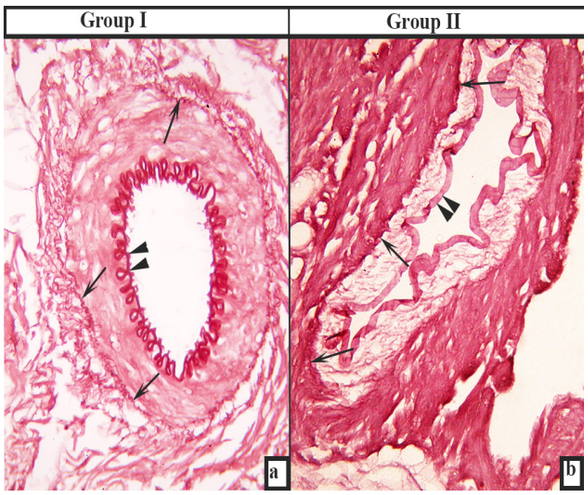

Fig. 14 (a&b): Photomicrographs of arcuate arteries of rabbit kidneys. [a] An arcuate artery of control group (I) showing a reddish-brown wavy internal elastic lamina (▲) in the intima and fine reddish-brown elastic fibers (↑) in the adventitia. [b] An arcuate artery of decellularization group (II) showing an intact and well preserved reddish-brown internal elastic lamina (▲) in the intima and fine reddish-brown elastic fibers (↑) in the adventitia. (Orcein x400)

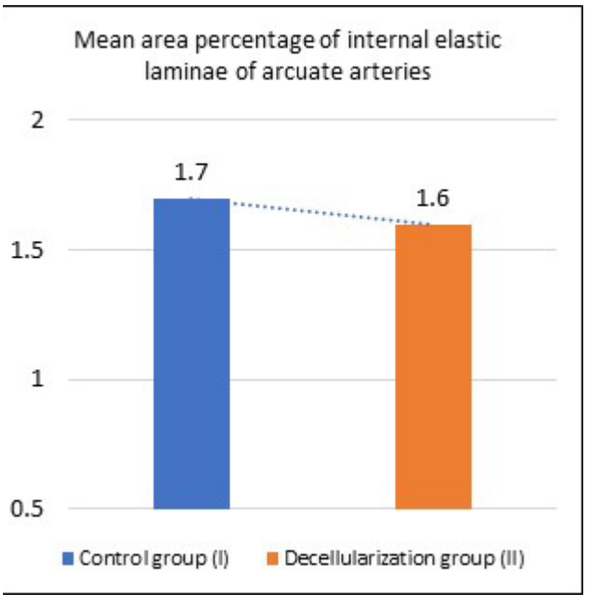

Fig. 15: A chart showing mean area percentage of internal elastic laminae of arcuate arteries of both control and decellularization groups.

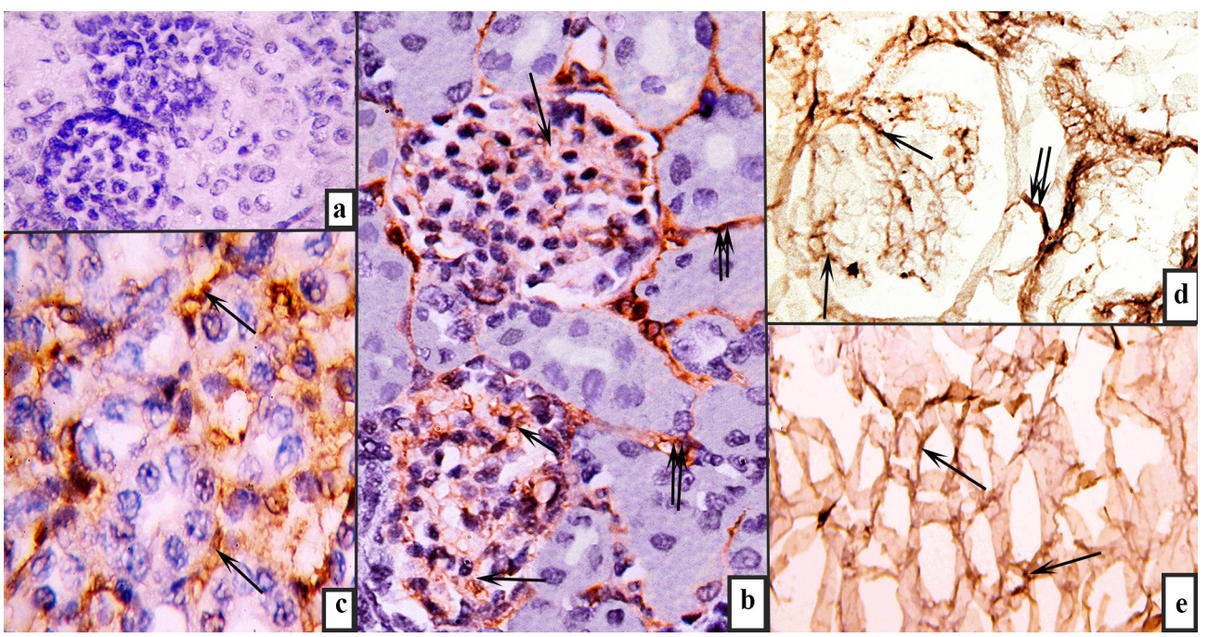

Fig. 16 (a:e): Photomicrographs of rabbit kidneys. [a] A negative control section of control group (I) showing no positive immunohistochemical reaction for laminin and no background staining. [b] Cortex of control group I showing positive immunohistochemical reaction for laminin in the GBMs (↑) and the basement membranes (↑↑) of convoluted tubules. [c] Medulla of control group I showing positive immunohistochemical reaction for laminin in basement membranes of medullary tubules and ducts (↑). [d] Cortex of decellularization group II showing positive immunohistochemical reaction for laminin in the GBMs (↑) and the basement membranes of convoluted tubules (↑↑). [e] Medulla of decellularization group II showing positive immunohistochemical reaction for laminin in basement membranes of medullary tubules and ducts (↑). (Anti-laminin antibody x1000)

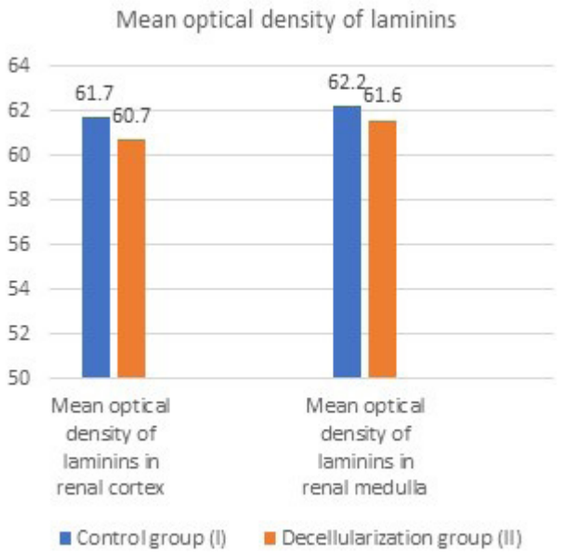

Fig. 17: A chart showing mean optical density of laminins in both renal cortex and medulla of both control and decellularization groups.

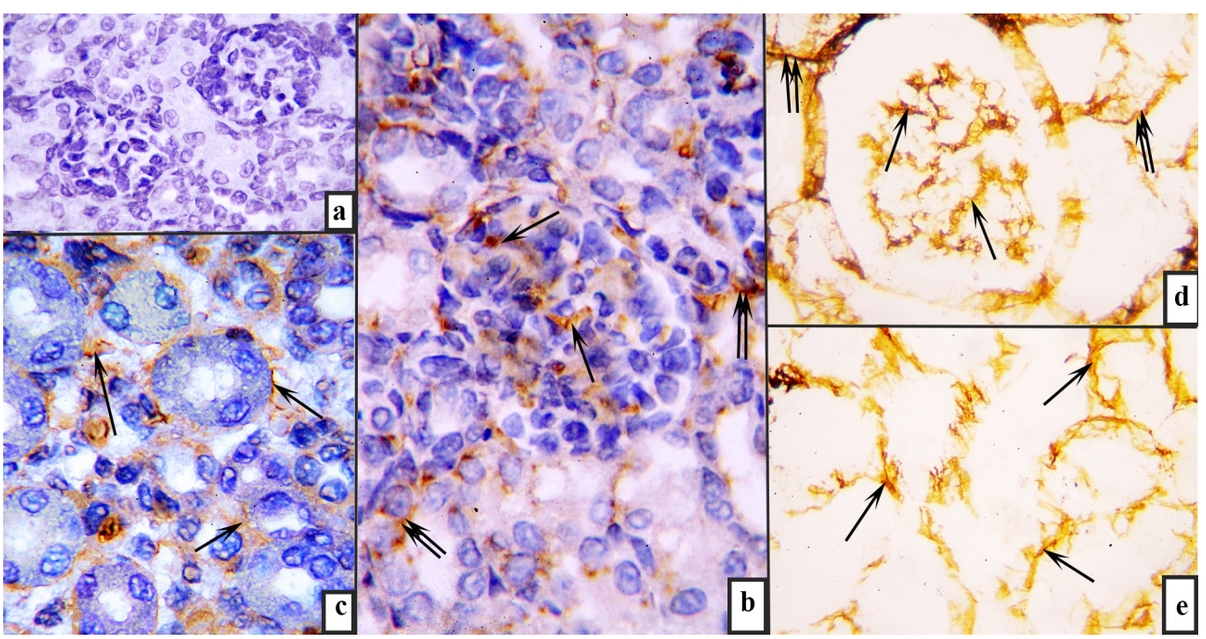

Fig. 18 (a:e): Photomicrographs of rabbit kidneys. [a] A negative control section of control group (I) showing no positive immunohistochemical reaction for fibronectin and no background staining. [b] Cortex of control group I showing positive immunohistochemical reaction for fibronectin in the GBMs and the mesangium (↑) and in the tubulointerstitium (↑↑). [c] Medulla of control group I showing positive immunohistochemical reaction for fibronectin in the tubulointerstitium (↑). [d] Cortex of decellularization group II showing positive immunohistochemical reaction for fibronectin in the GBMs and the mesangium (↑) and in the tubulointerstitium (↑↑). [e] Medulla of decellularization group II showing positive immunohistochemical reaction for fibronectin in the tubulointerstitium (↑). (Anti-fibronectin antibody x1000)

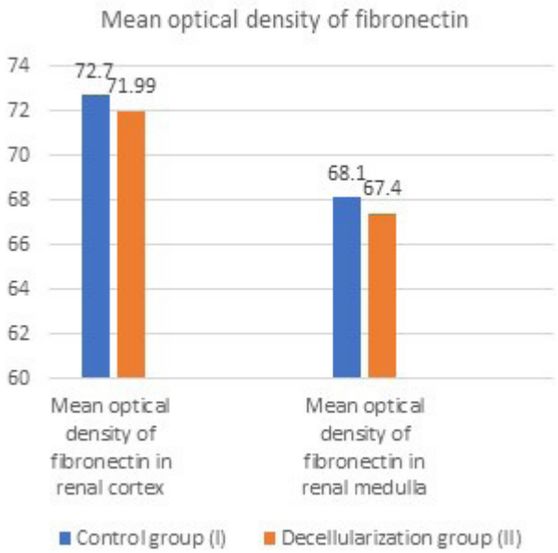

Fig. 19: A chart showing mean optical density of fibronectin in both renal cortex and medulla of both control and decellularization groups.

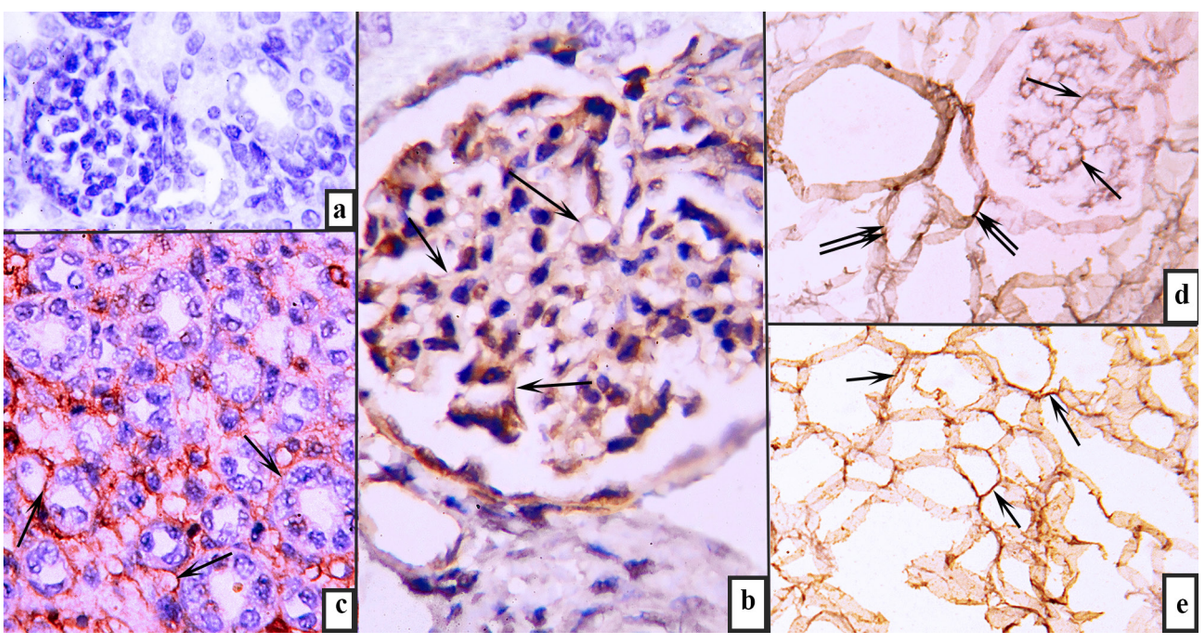

Fig. 20 (a:e): Photomicrographs of rabbit kidneys. [a] A negative control section of control group (I) showing no positive immunohistochemical reaction for collagen IV and no background staining. [b] Cortex of control group I showing positive immunohistochemical reaction for collagen IV in the GBMs (↑). [c] Medulla of control group I showing positive immunohistochemical reaction for collagen IV in basement membranes of medullary tubules and ducts (↑). [d] Cortex of decellularization group II showing positive immunohistochemical reaction for collagen IV in the GBMs (↑) and the basement membranes of convoluted tubules (↑↑). [e] Medulla of decellularization group II showing positive immunohistochemical reaction for collagen IV in basement membranes of medullary tubules and ducts (↑). (Anti-collagen IV antibody x1000)

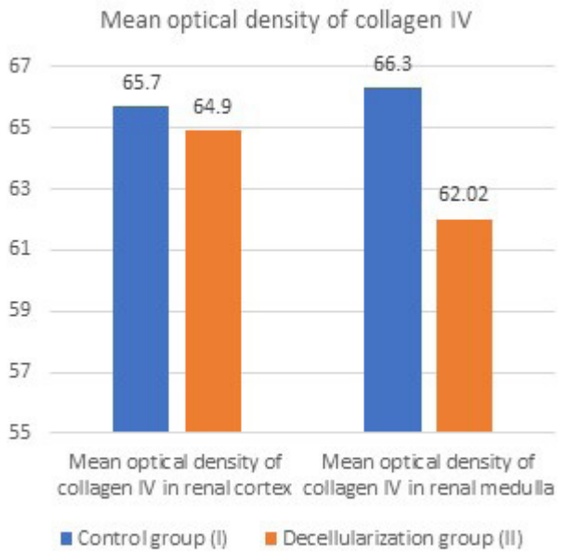

Fig. 21: A chart showing mean optical density of collagen IV in both renal cortex and medulla of both control and decellularization groups.

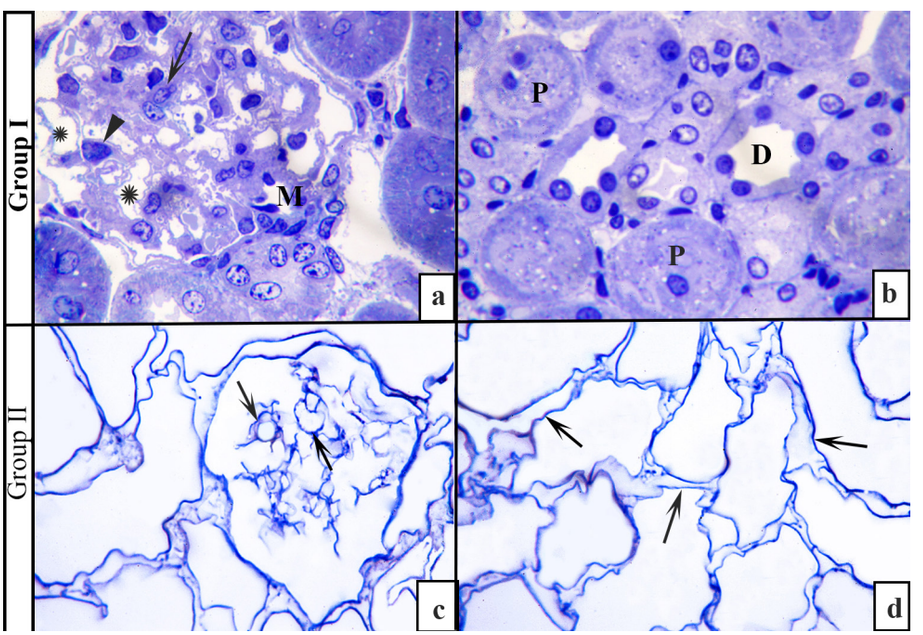

Fig. 22 (a:d): Photomicrographs of semithin section of rabbit kidney cortex. [a] Cortex of control group I showing a renal corpuscle surrounded by profiles of renal convoluted tubules. Glomerular capillaries (*) are seen surrounded by podocytes (▲) with mesangial cells in between (↑). The macula densa (M) is seen where the cells of DCT are crowded near the vascular pole of the glomerulus. [b] Cortex of control group I showing different profiles of renal convoluted tubules. PCTs are larger in diameter with narrower lumina, lined with fewer cells with apical brush borders almost masking their lumina. [c] Cortex of decellularization group II showing a renal corpuscle surrounded by profiles of renal convoluted tubules. Glomerular capillaries (↑) are seen intact with patent lumina. [d] Cortex of decellularization group II showing profiles of convoluted tubules with intact basement membranes (↑) and complete loss of their lining cells. PCTs & DCTs cannot be differentiated from each other. (Toluidine Blue x1000)

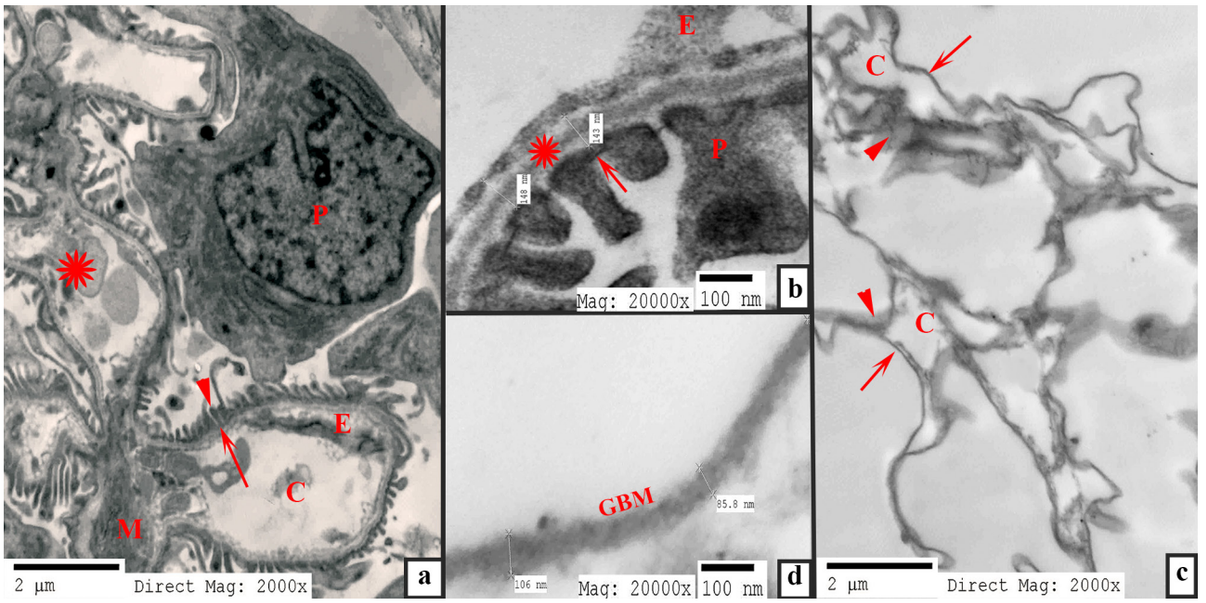

Fig. 23 (a:d): Photomicrographs of ultrathin sections of rabbit kidney cortex. [a] Cortex of control group I showing part of a renal corpuscle. Glomerular capillaries (C) are seen lined by flat endothelial cells (E) that may contain RBCs (*). The endothelial cells (E) rest on the GBM (↑) which is shared between several capillaries and is discontinuous where mesangium (M) is present. Note a podocyte (P) and its foot processes (▲) covering the outer side of the GBM. [b] Cortex of control group I showing the trilaminar GBM -two electron lucent laminae rara with a lamina densa in between (*)- formed by fusion of both basal laminae of endothelial cells (E) and podocytes foot processes (P). Filtration slit pores bridged by filtration slit diaphragms (↑) are seen between the interdigitating foot processes (P). [c] Cortex of decellularization group II showing glomerular capillaries (C) with patent lumina and intact GBMs (↑) with complete loss of lining cells. The capillaries are seen surrounded by mesangial matrix (▲). [d] Cortex of decellularization group II showing that the trilaminar appearance of GBM cannot be seen clearly. (TEM [a]& [c] x2000, [b]& [d] x20,000)

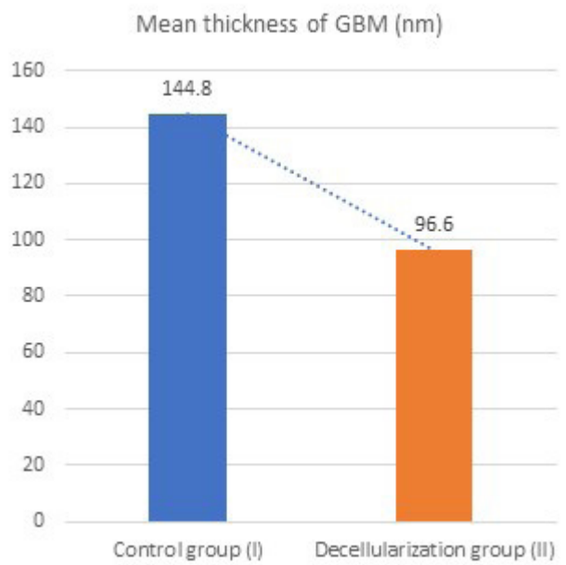

Fig. 24: A chart showing mean thickness of GBMs of both control and decellularization groups.

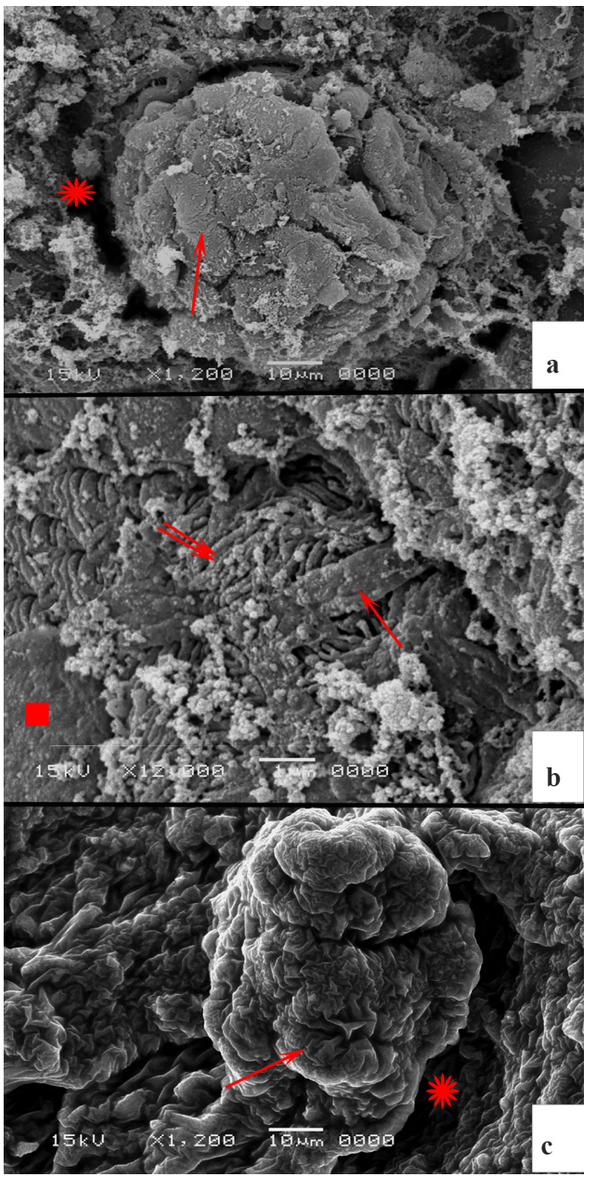

Fig. 25: Photomicrographs of rabbit kidney cortex. [a] Cortex of control group I showing a glomerulus formed of capillary loops (↑) surrounded by Bowman's/urinary space (*). [b] A higher magnification of the previous figure showing a podocyte cell body (■) extending complex primary processes, secondary processes (↑) and fine interdigitating tertiary processes (↑↑) covering the entire capillary surfaces. [c] Cortex of decellularization group (II) showing a glomerulus formed of intact capillary loops (↑) surrounded by Bowman's space (*). (SEM [a]& [c] x1200, [b] x12,000)

DISCUSSION

Kidney transplantation is an efficient lifesaving treatment for ESRD. Regrettably, kidney transplantation is limited worldwide by scarcity of organ donation, the growing waiting list for transplantation, graft failure and complications of immunosuppression[18]. Hopefully, Whole organ decellularization is an evolving technique for preparation of a 3D natural scaffold ready for recellularization with patient's own cells to produce a functioning kidney eligible for transplantation with minimal chance of being rejected[10]. Decellularization involves removal of the native cells present in a certain tissue while partially preserving the ECM proteins[7,9]. All methods of decellularization (chemical, physical, enzymatic and combinative) leads to disruption of the ECM proteins to some extent. The optimal decellularization protocol should create balance between the destructive effect of the decellularization method and preservation of the structural and mechanical properties of the resultant dECM[8,19]. Moreover, choosing the most suitable decellularization method is affected by tissue thickness, cell density, ECM density and tissue geometry. Hence, there is no general decellularization protocol for all tissue types[19]. The main objective of the current experiment was to present a decellularization protocol of male rabbit kidney and to characterize the resultant dECM by evaluating the structural integrity of its components.

In the current study, the left kidneys were chosen to be the decellularization group kidneys because they were easier to cannulate than the right ones. The liver on the right side covered the cranial pole of the right kidney. Also, the left renal artery was reported to be longer than the right renal artery[20].

A combination of physical and chemical decellularization methods were used in the presented protocol to complement the decellularizing effect of each other. Accordingly, prolonged exposure to their ECM destructive effect would be avoided. First, we performed a single freezing and thawing cycle as a physical decellularization method. Crapo *et al*., (2011) reported that freezing and thawing causes cell lysis with minimal loss of ECM proteins. But, multiple freezing and thawing cycles cause ECM disruption[21]. That's why in the presented study, we used a single cycle to cause the cell lysis while avoiding the ECM disruption. Another drawback is that cell remnants were still trapped within the kidney tissue and needed a subsequent method to flush them out. For that, we chose vascular perfusion technique to deliver our chemical decellularization agent of choice (SDS). Vascular perfusion exploits the native vasculature to deliver SDS solution to every single cell within the kidney tissue[12]. The renal artery was the (In) portal through which SDS solution was perfused. The renal vein was the (Out) portal through which the perfusate plus the cell remnants were drained leaving behind a completely semi- transparent white dECM with a visible arborization of the vascular tree. These gross observations and interpretations were confirmed by analysis of weight data. There was a non-significant decrease in mean kidney weight after the freezing and thawing, while there was a highly significant decrease in mean kidney weight after kidney decellularization perfusion due to removal of cell remnants.

The glomeruli are very delicate structures that were subjected to rupture because of the uncontrolled perfusion pressure, therefore in the present study we had to control the perfusion pressure by using a peristaltic pump that controlled the perfusion rate. We started with a low

perfusion rate. As the process of cell lysis was going on, the vascular resistance decreased. So, we gradually increased the perfusion rate to compensate the decreased resistance and to force the SDS to pass through the higher resistant and more dense regions. But, we were keen to keep the perfusion rate within physiological range of rabbit kidney blood flow 5.49±0.71 mL/min/g kidney[22] all the time. Similarly, Poornejad *et al*., (2016a) used incremental increases in flow rate while controlling the perfusion pressure not to exceed the normal pressure of porcine kidney. They reported removing 99% of the genetic material while preserving the microstructure of the resultant dECM scaffold[23].

The surface-active agent, SDS is the most widely used surfactant in household cleaners, personal care products, cosmetics, paints and varnishes[24,25]. It is also used as a protein denaturing agent in SDS-polyacrylamide gel electrophoresis. Also, SDS is considered a more effective detergent than other detergents as Triton-X100. Thus, it is widely used as a decellularizing agent of dense tissues and complex organs as the kidney[24]. SDS is amphiphilic; each molecule has a polar hydrophilic head and along hydrophobic hydrocarbon tail. In aqueous media, when the SDS molecules reach a critical concentration called critical micelle concentration (CMC), they aggregate into ball shaped micelles where the polar heads faces the water molecules, while the hydrophobic tails are hidden in the center away from water[26]. SDS disrupts the structure of cell membrane by attacking membrane lipids and proteins. The three-stage model explains how SDS solubilizes the membrane lipid bilayer. Stage (I) represents the first interaction between SDS and the outer monolayer of the lipid bilayer where the amphiphilic SDS molecules integrate themselves between the amphiphilic phospholipid molecules. Stage (II) starts when the SDS molecules reach the CMC; the outer monolayer is now saturated by them. The SDS molecules are curvophilic meaning that they tend to spontaneously self-assemble forming curves. On the contrary, phospholipid molecules are straight and tend to self-assemble forming flat surfaces. This leads to expansion and bending of the outer monolayer but not the inner monolayer because SDS is a slow solubilizing surfactant that cannot penetrate fast enough to the inner monolayer. Bending of the outer monolayer outward creates small membrane blebs that pinch off as phospholipid- protein-detergent mixed unilamellar micelles. Disintegration of the outer monolayer facilitates further penetration of SDS molecules through the inner layer leading to complete solubilization of the membrane bilayer. Stage (III) occurs due to interaction of the mixed micelles with more detergent molecules leading to breaking them down into smaller mixed micelles. These newer small micelles have a higher detergent/phospholipid or a higher detergent/protein ratio[27].

Regarding proteins, SDS is a strong protein denaturant. SDS cleavages the non-covalent bonds responsible for the native conformation of proteins. SDS can denature membrane, cytoplasmic and ECM proteins. Moreover, SDS is a negatively charged ionic surfactant that gives a net negative charge to those denaturated proteins[28]. Unfortunately, those ECM proteins are critical key factors during recellularization. Cytotoxicity of SDS and its difficulty of being washed out from tissues are other drawbacks of using SDS. This can impair the cytocompatibility of the dECM with the reseeded cells during recellularization[29]. Thus, in the current study, we focused on using a single surfactant (SDS) with the lowest possible concentration (0.5%) for the lowest possible duration (5-6 hours) to balance between completely decellularizing the male rabbit kidney while preserving the integrity of its ECM proteins. SDS was the most extensively used agent for kidney decellularization from different species at different concentrations (0.1%: 4%) and durations (few hours: days); either alone or in combination with other agents[30,31,32,33]. Also, there was no universal standardized assessment guidelines to evaluate the efficiency of those decellularization protocols and to evaluate their impact on the dECM. Herein, in the presented study, we systematically compare between cortex and the medulla of both the control and decellularization groups regarding complete removal of cellular and genetic material, preservation of dECM components (e.g. collagen, fibronectin, laminin and GAGs) and preservation of continuity and integrity of dECM.

In the current study, H&E examination of decellularization group exhibited an apparently preserved architecture of kidney tissue through the entire kidney regions (capsule, cortex, medulla, renal pelvis and vasculature) compared to the control group. Also, there was a universal and complete loss of nuclear basophilia. Similarly, Caralt *et al*., (2015) reported complete loss of nuclear basophilia and preserved architecture of dECM of rat kidney using (1% Triton X-100 for 20h followed by 0.1% SDS for 3 h, 20 min)[34].

Feulgen nuclear reaction examination in the presented protocol revealed complete loss of genetic material in both cortex and medulla of decellularization group compared to control group. Feulgen staining is still considered the gold standard for exact deoxyribonucleic acid (DNA) image cytometry[35]. The reaction is stoichiometric and is proportionate to DNA content within the nucleus[36].

Other DNA detection methods were reported in the literature. Bonandrini *et al*., (2014) used DAPI (Diamidino-phenylindole dihydrochloride) fluorescent staining and confirmed complete DNA removal from rat dECM produced by their protocol (1% SDS for 17 h at 0.4 mL/min)[37]. Furthermore, He *et al*., (2017) compared between different SDS concentration (0.125%:1%) and durations (4h &8h). They used Picogreen dsDNA assay kit to quantify precisely the residual DNA amount within each dECM. Less than 0.02% of DNA remained within all of dECMs[39]. In addition, Schmitt *et al*., (2017) used SYBR® Green fluorescent stain and confirmed complete DNA loss from rat dECM produced by their protocol (0.66% SDS for 60 min at 5mL/min)[38].

In the current study, Modified Masson′s trichrome examination revealed that amount and distribution of collagen fibers were preserved in both cortex and medulla of dECM of decellularization group when compared to control group. similarly, Peloso *et al*., (2015a) reported no significant difference between the native and decellularized rat kidneys by using Masson′s trichrome to examine collagen fibers. Their protocol used 100 mL of 1% Triton X-100 followed by 100 mL of 1% SDS at 70 mL/h. Furthermore, they used a collagen assay kit to quantify collagen spectrophotometrically[40]. The collagen family plays a critical role in tissue development; they are responsible for tensile strength, tissue support, endothelial cell movement during angiogenesis, cell adhesion, basal lamina formation and cell signaling[36].

In the presented study, Gordon & Sweets' silver impregnation examination revealed preservation of reticular fibers in both cortex and medulla of dECM compared to control group. In accordance with our results, Tajima *et al*., (2020) used periodic acid methenamine silver staining which showed preservation of basement membrane or reticular fibers around the glomeruli of beagle dog dECM produced by using 0.5% SDS at 15mL/min for 6h[41]. Reticular fibers- those delicate branching network forming type III collagen fibrils- provide a support system for cells while permitting easy diffusion of metabolites and some motility[15].

Orcein stain was used in the current study, to evaluate the integrity of elastic fibers as a part of the integrity of the entire vascular tree. Orcein stained section showed preservation of elastic fibers and internal elastic laminae in vascular walls of decellularization group same as control group. On the other hand, Zambon *et al*., (2018) used fluoroscopic angiography and made vascular corrosion casts followed by SEM imaging of these casts. Also, they performed re-endothelialization of the dECM scaffolds followed by in *vitro* blood transfusion. All these methods confirmed that their protocol (1% TritonX-100+ 0.5% SDS) preserved the integrity, endurance and patency of the dECM microvasculature[42].

Examination of PAS stained sections in this study showed preservation of density and distribution of glycoproteins and preservation of the integrity and continuity of basement membranes of dECM of both cortex and medulla compared to control kidney. The mean optical density of PAS positive reaction was chosen for analysis instead of the mean area percentage of glycoproteins because the latter was expected to decrease due to loss of cell membrane attached glycoproteins. Chani *et al*., (2017) used PAS staining which showed well preserved and uniformly stained glycoproteins in dECM of cryostored and freshly isolated kidneys[43]. Glycoproteins regulate cell movement, migration, proliferation and differentiation[36].

In the current study, combined Alcian blue- PAS stained section examination showed preservation of density and distribution GAGs present in ECM of both cortex and medulla of dECM compared to control kidney. Similar to glycoproteins, loss of cell membrane attached GAGs was expected. So, mean optical density of GAGs was used for analysis instead of their mean area percentage. Similarly, Peloso *et al*., (2015.a) used Alcian blue which confirmed the preservation of GAGs in cortex and medulla of the dECM[40]. Also, Chani *et al*., (2017) used Alcian blue and showed that GAGs of dECM was not affected by the decellularization process nor the cryostorage[43]. He *et al*., (2017) used Blyscan GAGs quantification assay to compare between multiple SDS concentrations and durations. They found that SDS diminished GAGs within the resultant dECM of all protocols. But, the 4-hour protocols preserved more GAGs than the 8-hour protocols. Also, the 0.125% SDS for 4 hours protocol (lowest duration and concentration of SDS) showed the highest preservation of GAGs[39]. GAGs provide hydration, force resistance and structural support for the ECM[15]. They also act as a reservoir for growth factors as tissue growth factor-ß (TGF-ß) and fibroblast growth factor (FGF). GAGs contribute to the net negative charge of the GBM, cell to cell and cell to ECM interactions[44].

In the current study, immunohistochemical examination of laminin and fibronectin revealed preservation of their density and distribution in both cortex and medulla of decellularized kidneys compared to control kidney. Similar finding were reported by Peloso *et al*., (2015a) who used immunofluorescence examination for both laminin and fibronectin that showed preservation of both of them in cortex and medulla of dECM[40]. Similarly, Schmitt *et al*., (2017) reported preservation of both laminin and fibronectin even when applying the harshest decellularization protocol (1% SDS for 120 min at 5mL/min followed by 5 hours wash with PBS) in their comparative study[38]. Laminin has a critical role in the assembly of the basal lamina suprastructure through interaction with collagen type IV. Also, it is involved in cell signaling, tissue development, differentiation and remodeling[36]. Fibronectin has multiple binding sites for different ECM components (collagens, laminin, GAGs, fibronectin) leading stabilization of the ECM. Also, fibronectin has a binding site for integrins playing a role in cell attachment to ECM[45]. Furthermore, many growth factors have been identified to have binding sites on fibronectin as FGF, vascular endothelial growth factor (VEGF) and platelet derived growth factor (PDGF). Thus, fibronectin is considered a growth factors reservoir and a regulator of their intensity and duration of signaling. Accordingly, it controls cell behavior, polarity, survival, differentiation, proliferation, and migration[46].

In addition, Immunohistochemical examination of Collagen type IV in the presented study revealed that collagen type IV was preserved in the cortex of the dECM, but it was significantly affected in the renal medulla of dECM compared to control group. Similarly, He *et al*., (2017) used immunohistochemistry to evaluate integrity of both collagen type I and IV. But, they reported preservation of both collagen types in all protocols they have been comparing[39]. Also, Xue *et al*., (2018) used immunohistochemistry to demonstrate that their

decellularization protocol (0.5% SDS at 0.5 mL/min for 8 hours) resulted in similar distribution of collagen IV compared to the control kidney[47]. Collagen type IV represents the most abundant structural protein of all basement membranes. Also, it represents a cell signaling platform through interaction with integrins[48].

Glomeruli and renal tubules are very delicate structures prone to damage due to high perfusion pressure and SDS that denature their scaffolding proteins. TEM examination in the current study confirmed complete cell removal and preservation of the continuity of GBMs and tubular basement membranes. But, both laminae rara externa and interna of GBM were disrupted and the GBM thickness was decreased significantly. In accordance with our work, TEM was used by Xue *et al*., (2018) who confirmed removal of all cellular components while the continuity of basement membranes were still intact.

In current study, SEM examination showed preservation of the 3D structure of glomeruli and renal tubules. SEM examination was also used by Xue *et al*., (2018) who reported preservation of the 3D structure of the decellularized scaffold[47]. In addition, Hu *et al*., (2020) reported that their protocol preserved the native globular and tubular stereostructures of the rat dECM[49].

CONCLUSION

The presented protocol demonstrated efficient decellularization of male rabbit kidney while preserving the integrity of the dECM; most structural components, the ultrastructure and the 3D structure. Thus, it could represent a promising protocol for preparing a natural dECM scaffold ready for engineering a whole kidney. Further studies are needed to evaluate its capability to support cell growth and differentiation during recellularization. Also, further studies are needed to confirm in *vivo* loss of the resultant dECM immunogenicity and to evaluate the in *vivo* vascular patency in order to confirm whether the resultant dECM can resist the arterial blood pressure or not.

ABBREVIATIONS

ECM: Extracellular matrix; **dECM:** Decellularized extracellular matrix; **NZWR:** New Zealand White Rabbits; **SDS:** Sodium dodecyl sulfate; **3D:** Three-dimensional; **CKD:** Chronic kidney disease; **ESRD:** End stage renal disease; **IV:** Intravenous/ intravenously; **PBS:** Phosphate buffered saline; **PAS:** modified McManus periodic acid Schiff's technique; **TEM:** Transmission electron microscope; **SEM:** Scanning electron microscope; **GAGs:** Glycosaminoglycans; **GBM/s:** Glomerular basement membrane/s; **P:** probability of chance; **H&E:** Hematoxylin and Eosin; **PCTs:** proximal convoluted tubules; **DCTs:** distal convoluted tubules; **CMC:** critical micelle concentration; **DAPI:** Diamidino-phenylindole dihydrochloride; **DNA:** deoxyribonucleic acid; **TGF-ß:** tissue growth factor-ß; **FGF:** fibroblast growth factor; **VEGF:** vascular endothelial growth factor; **PDGF:** platelet derived growth factor.

CONFLICT OF INTERESTS

There are no conflicts of interest.

REFERENCES

1. Levin A, Stevens PE, Bilous RW, Coresh J, De Francisco ALM, De Jong PE, Griffith KE, Hemmelgarn BR, Iseki K, Lamb EJ, Levey AS, Riella MC, Shlipak MG, Wang H, White CT, Winearls CG. Kidney disease: Improving global outcomes (KDIGO) CKD work group. KDIGO 2012 clinical practice guideline for the evaluation and management of chronic kidney disease. Kidney International Supplements. 2013;3(1):1-150. doi:10.1038/kisup.2012.73.

2. Levin A. Improving global kidney health: International society of nephrology initiatives and the global kidney health atlas. Annals of Nutrition and Metabolism. 2018;72(2):28-32. doi:10.1159/000488123.

3. Luyckx VA, Tonelli M, Stanifer JW. The global burden of kidney disease and the sustainable development goals. Bulletin of the World Health Organization. 2018;96:414-422. doi:10.2471/BLT.17.206420.

4. United States Renal Data System. USRDS annual data report: Epidemiology of kidney disease in the United States. National Institutes of Health, National Institute of Diabetes and Digestive and Kidney Diseases, Bethesda, MD, 2018; 2: 291-702.

5. Bicalho PR, Requião-Moura LR, Arruda ÉF, Chinen R, Mello L, Bertocchi AP, Lamkowski Naka E, Tonato EJ, Pacheco-Silva A. Long-Term Outcomes among Kidney Transplant Recipients and after Graft Failure: A Single-Center Cohort Study in Brazil. BioMed research international. 2019; Volume 2019. Article ID 7105084 : p1-10. doi:10.1155/2019/7105084.

6. Murphy CM, O'Brien FJ, Little DG, Schindeler A. Cell-scaffold interactions in the bone tissue engineering triad. European cells & materials. 2013; 26: 120-132. doi:10.22203/eCM.v02609.

7. Destefani AC, Sirtoli GM, Nogueira BV. Advances in the Knowledge about Kidney Decellularization and Repopulation. Frontiers in bioengineering and biotechnology. 2017; 5(34): 1-28. doi:10.3389/fbioe.2017.00000.

8. Garreta E, Oria R, Tarantino C, Pla-Roca M, Prado P, Fernandez-Aviles F, Campistol JM, Samitier J, Montserrat N. Tissue engineering by decellularization and 3D bioprinting. Materials Today. 2017; 20(4):166-178. doi:10.1016/j.mattod.2016.12.005.

9. Gilpin A, Yang Y. Decellularization strategies for regenerative medicine: from processing techniques to applications. BioMed research international; 2017: 1-13. Article ID 9831534. doi:10.1155/2017/9831534.

10. Hillebrandt KH, Everwien H, Haep N, Keshi E, Pratschke J, Sauer IM. Strategies based on organ decellularization and recellularization. Transplant International. 2019; 32: 571–585. doi:10.1111/tri.13462.

11. Nakayama KH, Lee CC, Batchelder CA, Tarantal AF. Tissue specificity of decellularized rhesus monkey kidney and lung scaffolds. PloS one. 2013;8(5):1-10:e64134. doi:10.1371/journal.pone.0064134.

12. Taylor DA, Sampaio LC, Ferdous Z, Gobin AS, Taite LJ. Decellularized Matrices in Regenerative Medicine. Acta Biomaterialia. 2018; 74: 74–89. doi:10.1016/j.actbio.2018.04.044.

13. Flecknell P. Laboratory animal anaesthesia. Third edition. Amsterdam: Academic press; 2009.

14. Schmitt AJ, Wallner AK, Afazel S, Killer-Oberpfalzer M. Monitoring of the heparinization in the rabbit animal model during endovascular interventions. Neuroradiology. 2013; 55(7): 883-888. doi:10.1007/s00234-013-1189-y.

15. Suvarna KS, Layton C, Bancroft JD. Bancroft's Theory and Practice of Histological Techniques. Eighth edition. Elsevier; 2019.

16. McManus JF, Mowry RW. Staining Method: Histologic and Histochemical. USA: Paul B. Hoeber Inc, Medical Division of Harper & Brothers;1960.

17. Murtey MD, Ramasamy P. Sample preparations for scanning electron microscopy–life sciences. In: Janecek M, Kral R. (eds.) Modern electron microscopy in physical and life sciences. IntechOpen; 2016 :p.161-185. doi: 10.5772/61720.

18. Girlanda R. Deceased organ donation for transplantation: challenges and opportunities. World journal of transplantation. 2016; 6(3): 451-459. doi: 10.5500/wjt.v6.i3.451.

19. Keane TJ, Swinehart I, Badylak SF. Methods of tissue decellularization used for preparation of biologic scaffolds and in *vivo* relevance. Methods. 2015; 84: 25-34. doi:10.1016/j.ymeth.2015.03.005.

20. Santos-Sousa CA, Stocco AV, Mencalha R, Jorge SF, Abidu-Figueiredo M. Morphometry and Vascularization of the Rabbit Kidneys (Oryctolagus cuniculus). International Journal of Morphology. 2015; 33(4): 1293-1298. doi: 10.4067/S0717-95022015000400017.

21. Crapo PM, Gilbert TW, Badylak SF. An overview of tissue and whole organ decellularization processes. Biomaterials. 2011; 32(12): 3233-3243. doi:10.1016/j.biomaterials.2011.01.057.

22. Takami A, Yoshida K, Tadokoro H, Kitsukawa S, Shimada K, Sato M, Suzuki K, Masuda Y, Tanada S. Uptakes and Images of 38K in Rabbit Heart, Kidney, and Brain. 2000; 41(4):763-769.

23. Poornejad N, Momtahan N, Salehi AS, Scott DR, Fronk CA, Roeder BL, Reynolds PR, Bundy BC, Cook AD. Efficient decellularization of whole porcine kidneys improves reseeded cell behavior. Biomedical Materials. 2016a; 11(2): 025003. doi:10.1088/17486041/11/2/025003.

24. Niraula TP, Bhattarai A, Chatterjee SK. Sodium dodecylsulphate: A very useful Surfactant for Scientific Investigations. Journal of Knowledge and Innovation. 2014; 2(1): 111-113. ISSN: 2350-8884(P).

25. Wołowicz A, Staszak K. Study of surface properties of aqueous solutions of sodium dodecyl sulfate in the presence of hydrochloric acid and heavy metal ions. Journal of Molecular Liquids. 2020; 299:1-16. doi:10.1016/j.molliq.2019.112170.

26. Bhairi SM, Mohan C, Ibryamova S, LaFavor T. Detergents: A guide to the properties and uses of detergents in biological systems. EMD Millipore Corporation. Massachusetts, United States. 2017. https://www.sigmaaldrich.com/content/dam/sigma-aldrich/1/content/commerce/pdfs/detergents/detergents-guide-mk.pdf

27. Lichtenberg D, Ahyayauch H, Goñi FM. The mechanism of detergent solubilization of lipid bilayers. Biophysical journal. 2013; 105(2): 289-299. doi:10.1016/j.bpj.2013.06.007.

28. Stephenson FH. Protein. In: Calculations for molecular biology and biotechnology. Third edition. Amsterdam. Academic press; 2016. p. 375-429. doi:10.1016/B978-0-12-802211-5.00011-4.

29. Zambon JP, Atala A, Yoo JJ. Methods to generate tissue-derived constructs for regenerative medicine applications. Methods. 2020; 171: 3-10. doi:10.1016/j.ymeth.2019.09.016.

30. Ross EA, Williams MJ, Hamazaki T, Terada N, Clapp WL, Adin C, Ellison GW, Jorgensen M, Batich CD. Embryonic stem cells proliferate and differentiate when seeded into kidney scaffolds. Journal of the American Society of Nephrology. 2009; 20(11): 2338-2347. doi: 10.1681/ASN.2008111196.

31. Park KM, Woo HM. Porcine bioengineered scaffolds as new frontiers in regenerative medicine. Transplantation proceedings. 2012; 44 (4): 1146-1150. doi:10.1016/j.transproceed.2012.03.043.

32. Sullivan DC, Mirmalek-Sani SH, Deegan DB, Baptista PM, Aboushwareb T, Atala A, Yoo JJ. Decellularization methods of porcine kidneys for whole organ engineering using a high-throughput system. Biomaterials. 2012; 33(31): 7756-7764. doi: 10.1016/j.biomaterials.2012.07.023.

33. Hussein KH, Saleh T, Ahmed E, Kwak HH, Park KM, Yang SR, Kang BJ, Choi KY, Kang KS, Woo HM. Biocompatibility and hemocompatibility of efficiently decellularized whole porcine kidney for tissue engineering. Journal of Biomedical Materials Research Part A. 2018; 106(7): 2034-2047. doi: 10.1002/jbm.a.36407

34. Caralt M, Uzarski JS, Iacob S, Obergfell KP, Berg N, Bijonowski BM, Kiefer KM, Ward HH, Wandinger-Ness A, Miller WM, Zhang ZJ, Abecassis MM, Wertheim JA. Optimization and critical evaluation of decellularization strategies to develop renal extracellular matrix scaffolds as biological templates for organ engineering and transplantation. American journal of transplantation. 2015; 15(1): 64-75. doi:10.1111/ajt.12999.

35. Biesterfeld S, Beckers S, Cadenas MD, Schramm M. Feulgen staining remains the gold standard for precise DNA image cytometry. Anticancer research. 2011;31(1):53-58. PMID: 21273580.

36. Ross MH., Pawlina W. Histology: a text and atlas: with correlated cell and molecular biology. Seventh edition. Wolters Kluwer Health; 2016.

37. Bonandrini B, Figliuzzi M, Papadimou E, Morigi M, Perico N, Casiraghi F, Dipl C, Sangalli F, Conti S, Benigni A, Remuzzi A, Remuzzi G. Recellularization of well-preserved acellular kidney scaffold using embryonic stem cells. Tissue Engineering Part A. 2014; 20(9-10):1486-1498. doi: 10.1089/ten.tea.2013.0269.

38. Schmitt A, Csiki R, Tron A, Saldamli B, Tübel J, Florian K, Siebenlist S, Balmayor E, Burgkart R. Optimized protocol for whole organ decellularization. European journal of medical research. 2017; 22(31). doi 10.1186/s40001-017-0272-y

39. He M, Callanan A, Lagaras K, Steele JAM, Stevens MM. Optimization of SDS exposure on preservation of ECM characteristics in whole organ decellularization of rat kidneys. Journal of Biomedical Materials Research Part B: Applied Biomaterials. 2017; 105(6):1352-1360. doi: 10.1002/jbm.b.33668.

40. Peloso A, Ferrario J, Maiga B, Benzoni I, Bianco C, Citro A, Currao M, Malara A, Gaspari A, Balduini A, Abelli M, Piemonti L, Dionigi P, Orlando G, Maestri M. Creation and implantation of acellular rat renal ECM-based scaffolds. Organogenesis. 2015(a); 11(2):58-74. doi: 10.1080/15476278.2015.1072661.

41. Tajima K, Kuroda K, Otaka Y, Kinoshita R, Kita M, Oyamada T, Kanai K. Decellularization of canine kidney for three-dimensional organ regeneration. Veterinary World. 2020;13(3):452- 457. doi: 10.14202/vetworld.2020.452-457.

42. Zambon JP, Ko IK, Abolbashari M, Huling J, Clouse C, Kim TH, Smith C, Atala A, Yoo JJ. Comparative analysis of two porcine kidney decellularization methods for maintenance of functional vascular architectures. Acta biomaterialia. 2018; 75: 226-234. doi: 10.1016/j.actbio.2018.06.004.

43. Chani B, Puri V, Sobti RC, Jha V, Puri S. Decellularized scaffold of cryopreserved rat kidney retains its recellularization potential. PloS one. 2017; 12(3): e0173040.doi:10.1371/journal.pone.0173040.

44. Bülow RD, Boor P. Extracellular matrix in kidney fibrosis: more than just a scaffold. Journal of Histochemistry & Cytochemistry. 2019; 67(9): 643-661. doi:10.1369/002215541984938.

45. Farhat WA, Geutjes PJ. Artificial biomaterials for urological tissue engineering. In: Denstedt J, Atala A. (eds.) Biomaterials and Tissue Engineering in Urology. Woodhead Publishing; 2009 (p. 243-254). doi: 10.1533/9781845696375.3.243.

46. Zhu J, Clark RA. Fibronectin at select sites binds multiple growth factors and enhances their activity: expansion of the collaborative ECM-GF paradigm. Journal of Investigative Dermatology. 2014; 134(4): 895-901. doi:10.1038/jid.2013.484.

47. Xue A, Niu G, Chen Y, Li K, Xiao Z, Luan Y, Sun C, Xie X, Zhang D, Du X, Kong F, Guo Y, Zhang H, Cheng G, Xin Q, Guan Y, Zhao S. Recellularization of well-preserved decellularized kidney scaffold using adipose tissue-derived stem cells. Journal of biomedical materials research Part A. 2018; 106(3):805-814. doi: 10.1002/jbm.a.36279.

48. Tryggvason K, Patrakka J. Alport's disease and thin basement membrane nephropathy. In: Lifton RP, Somlo S, Giebisch GH, Seldin DW (eds.). Genetic Diseases of the Kidney. Academic Press; 2009 (p. 77-96). doi: 10.1016/B978-0-12-449851-8.00004-8.

49. Hu D, Zhang D, Liu B, Liu Y, Zhou Y, Yu Y, Shen L, Long C, Zhang D, Liu X, Lin T, He D, Xu T, Timashev P, Butnaru D, Zhang Y, Wei G. Human ucMSCs seeded in a decellularized kidney scaffold attenuate renal fibrosis by reducing epithelial–mesenchymal transition via the TGF-β/Smad signaling pathway. Pediatric Research. 2020; 88: 192–201. doi:10.1038/s41390-019-0736-6.

الملخص العربى

توصيف كلية ذكر الأرنب المنزوعة الخلايا كدعامة طبيعية ثلاثية الأبعاد في مجال هندسة الأنسجة، دراسة هستولوجية

سارة عبد الجواد،آيات عبد النبي، جيهان خلف، نجلاء أبو رابية

قسم الهستولوجيا وبيولوجيا الخلية. كلية الطب - جامعة عين شمس

المقدمة: إن زرع الكلى يعتبر العلاج الوحيد لمرض الفشل الكلوي في مراحله النهائية. يعد نقص الأعضاء المتبرع بها أحد العقبات العديدة التي تواجه زراعة الكلى. تقدم عملية إزالة الخلايا من كامل العضو سقالة طبيعية ثلاثية الأبعاد التي يمكن زرعها حيث تعتبر كلية جديدة متوافقة مع الجهاز المناعي وجاهزة للزرع. كان الهدف من هذه الدراسة هو توصيف الكلى منزوعة الخلايا من خلال تقييم السلامة الهيكلية للمطرس الخارج الخلوي باعتباره سقالة طبيعية جاهزة لهندسة الأنسجة.

المواد وطرق البحث: تم حصاد الكلى من عشرة ذكور من الأرانب البيضاء النيوزيلندية بمتوسط وزن ١٠٠٠ - ١٥٠٠ جم. المجموعة الأولى: المجموعة الضابطة وتضمنت الكُلى اليمنى العشر وقد تمت معالجتها على الفور للفحص النسيجي والفحص الكيميائي الهيستولوجي المناعي والفحص بالمجهر الإلكتروني. المجموعة الثانية :المجموعة المنزوعة الخلايا وتضمنت الكُلى اليسرى العشر. وقد تم حصادها بعناية بعد تركيب قنية وريدية تحت التخدير وتم حفظها مجمدة حتى بدء عملية إزالة الخلايا. فعندها تمت إذابة الكلى، وتم حقنها ب ٠,٥ ٪ كبريتات دوديسيل الصوديوم (اس دي اس) لمدة ٥ - ٦ ساعات في درجة حرارة الغرفة حتى أصبحت الكلى بيضاء تمامًا. أخيرًا، تمت معالجة الكلى منزوعة الخلايا للفحص النسيجي و الفحص الكيميائي الهيستولوجي المناعي و الفحص بالمجهر الإلكتروني.

النتائج: أسفر الفحص المجهرى عن إزالة الخلايا بالكامل من كلى المجموعة الثانية. كما تم الحفاظ على سلامة المكونات المختلفة للمطرس الخارج الخلوي و تم الحفاظ على المظهر النسيجي للعمارة الكلوية والحفاظ على البنية التحتية الدقيقة جيدًا.بينما ظهر انخفاض ملحوظ احصائيا لمتوسط الكثافة البصرية للكولاجين الرابع في النخاع الكلوي و انخفاض في سمك الأغشية القاعدية الكبيبية لمجموعة إزالة الخلايا عن المتوسط المسجل للمجموعة الضابطة.

الاستنتاج: مما سبق تم استنتاج أن البروتوكول المستخدم قام بكفاءة بإزالة الخلايا من كلية الأرانب الذكور. و من الممكن أن تمهد هذه النتائج الطريق لمزيد من التحقيقات للانتقال إلى الخطوة التالية "إعادة العزل الخلوي".